USAAMRDL-TR-75-41

ELASTIC PITCH BEAM TAIL ROTOR FOR LOH

Kaman Aerospace Corporation
Bloomfield, Conn. 06002

July 1976

Final Report

Prepared for

EUSTIS DIRECTORATE
U. S. ARMY AIR MOBILITY RESEARCH AND DEVELOPMENT LABORATORY
Fort Eustis, Va. 23604

EUSTIS DIRECTORATE POSITION STATEMENT

This report presents a reasonable design concept for an elastic pitch beam tail rotor for the LOH class of helicopters. Incorporation of a removable/replaceable airfoil and the elimination of the pitch bearings and simplified hub enhance the reliability and maintainability of the tail rotor and hub assembly. Elimination of the teeter bearing, however, does produce higher vibratory hub moments to be reacted by the tail rotor shaft. The results of the UH-1 elastic pitch beam tail rotor program provide the base technology for future application of this concept on production helicopters.

Mr. James P. Waller of the Technical Applications Division served as project engineer for this effort.

UNCLASSIFIED

SECURITY CLASSIFICATION OF THIS PAGE (When Data Entered)

REPORT DOCUMENTATION PAGE

READ INSTRUCTIONS BEFORE COMPLETING FORM

1. REPORT NUMBER: USAAMRDL-TR-75-41	2. GOVT ACCESSION NO.
3. RECIPIENT'S CATALOG NUMBER	
4. TITLE (and Subtitle): ELASTIC PITCH BEAM TAIL ROTOR FOR LOH,	5. TYPE OF REPORT & PERIOD COVERED: Final Rept.,
6. PERFORMING ORG. REPORT NUMBER: R-1332	
7. AUTHOR(s): John D. Porterfield, Frank B. Clark	8. CONTRACT OR GRANT NUMBER(s): DAAJ02-73-C-0073 New
9. PERFORMING ORGANIZATION NAME AND ADDRESS: Kaman Aerospace Corporation, Bloomfield, Connecticut 06002	10. PROGRAM ELEMENT, PROJECT, TASK AREA & WORK UNIT NUMBERS: 63204A 1F163204DB38 00 016 EK
11. CONTROLLING OFFICE NAME AND ADDRESS: U.S. Army Air Mobility Research & Development Laboratory, Eustis Directorate, Fort Eustis, Virginia 23604	12. REPORT DATE: July 1976 — 13. NUMBER OF PAGES: 87 — 89 p.
14. MONITORING AGENCY NAME & ADDRESS (if different from Controlling Office)	15. SECURITY CLASS. (of this report): Unclassified
	15a. DECLASSIFICATION/DOWNGRADING SCHEDULE

16. DISTRIBUTION STATEMENT (of this Report)

Approved for public release; distribution unlimited.

17. DISTRIBUTION STATEMENT (of the abstract entered in Block 20, if different from Report)

DA-1-F-163204-DB-38

18. SUPPLEMENTARY NOTES

1-F-163204-DB-3800

19. KEY WORDS (Continue on reverse side if necessary and identify by block number)

Helicopter rotors
Composite material
Structures
OH-58A

20. ABSTRACT (Continue on reverse side if necessary and identify by block number)

This report uses the results of Contract DAAJ01-73-C-0282(P3L), Elastic Pitch Beam Tail Rotor Study for LOH Class Helicopters, and Contract DAAJ02-72-C-0006, Elastic Pitch Beam Tail Rotor, for selecting the most promising concepts to establish detailed designs that are applicable to LOH class helicopters. The designs studied herein included removable/replaceable blade airfoil shells, damage/erosion-resistant leading edge, and damage tolerant/repairable trailing edge. The elimination of bearings →

DD FORM 1 JAN 73 1473 EDITION OF 1 NOV 65 IS OBSOLETE

UNCLASSIFIED

SECURITY CLASSIFICATION OF THIS PAGE (When Data Entered)

404362

4/B

20. (Cont'd)

was an important design objective; where bearings were required, consideration was given to the use of elastomeric bearings. Improvements in reliability and maintainability, repairability, cost, performance and producibility along with interchangeability with existing tail rotor systems were also prime considerations in the design selection.

PREFACE

This report was prepared by Kaman Aerospace Corporation of Bloomfield, Connecticut, for the Eustis Directorate, U.S. Army Mobility Research and Development Laboratory, Fort Eustis, Virginia, under contract DAAJ02-73-C-0073. Mr. James P. Waller was the contract monitor for the Army.

Kaman Aerospace Corporation personnel engaged in this program were John D. Porterfield and Paul F. Maloney of the Stress Department; Frank B. Clark, Material and Process Engineer; and Harry A. Cooke of the Research Department.

TABLE OF CONTENTS

LIST OF ILLUSTRATIONS

LIST OF TABLES

INTRODUCTION

High maintenance requirements, low reliability, and marginal performance are terms that have been frequently applied to current helicopter tail rotors. High rotational speeds, complex and variable inflow causing unique aerodynamic and dynamic loading conditions, and a susceptibility to failure from inherent causes as well as to foreign object damage and erosion are indicative symptoms of the tail rotor's hostile environment. Results of previous studies reported in References 1, 2 and 3 have indicated the feasibility of utilizing the Elastic Pitch Beam concept to design and fabricate tail rotors having maintainability, reliability and performance that are improved over current designs. The elimination of high oscillatory rate teeter or flapping bearings, the elimination of highly loaded pitch bearings, the use of damage-resistant and erosion-resistant materials, and the simplification of the hub details are some of the features that may be incorporated in the design of an Elastic Pitch Beam tail rotor to attain the desired improvements.

The Elastic Pitch Beam concept is used in this program to design a tail rotor for LOH class helicopters, in particular, the OH-58A, Figure 1. Several Elastic Pitch Beam tail rotor design configurations for both the OH-58A and OH-6A helicopters were investigated in Reference 3 to establish the most promising concepts warranting further study. Conclusions reached in the Reference 3 study indicated that the Elastic Pitch Beam tail rotor defined as Configuration A for the OH-58A, shown in Figure 2, would be the most favorable candidate for follow-on investigations leading to a flight-worthy, cost-effective tail rotor system for an LOH class helicopter. In view of this, the work accomplished under this contract was concentrated on developing an Elastic Pitch Beam tail rotor that could be interchangeably mounted on the OH-58A helicopter.

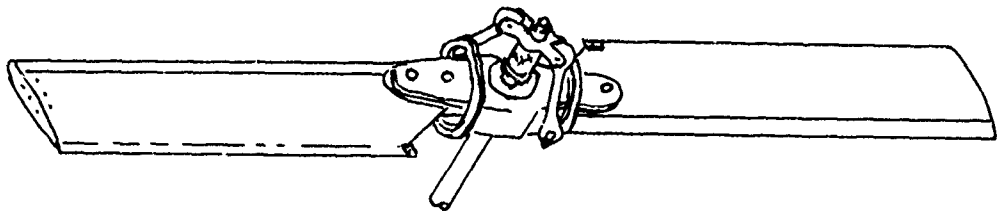

Figure 1. Current OH-58A Tail Rotor.

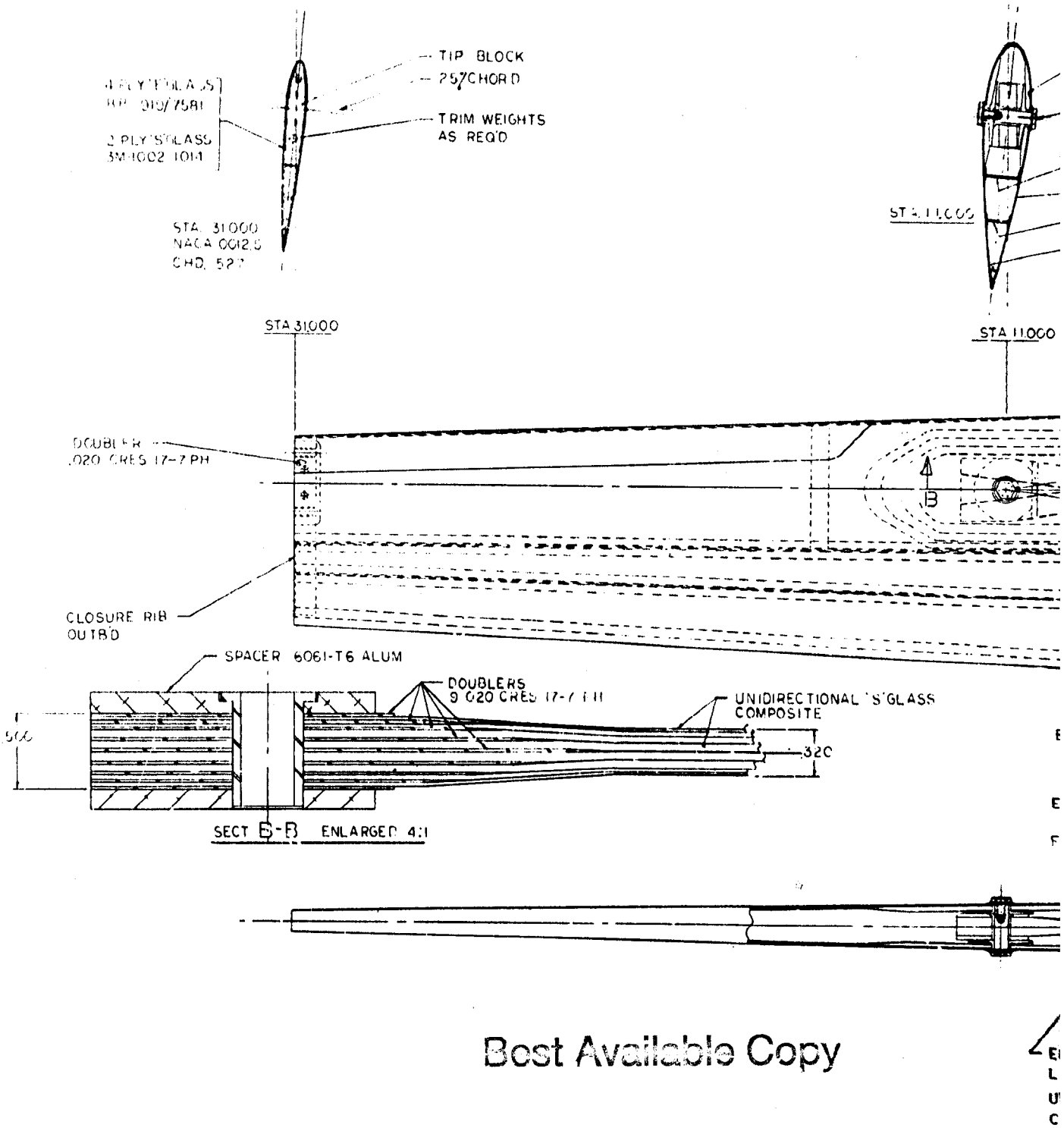

Figure 2. LOH Elastic Pitch Beam Tail Rotor, OH-58A.

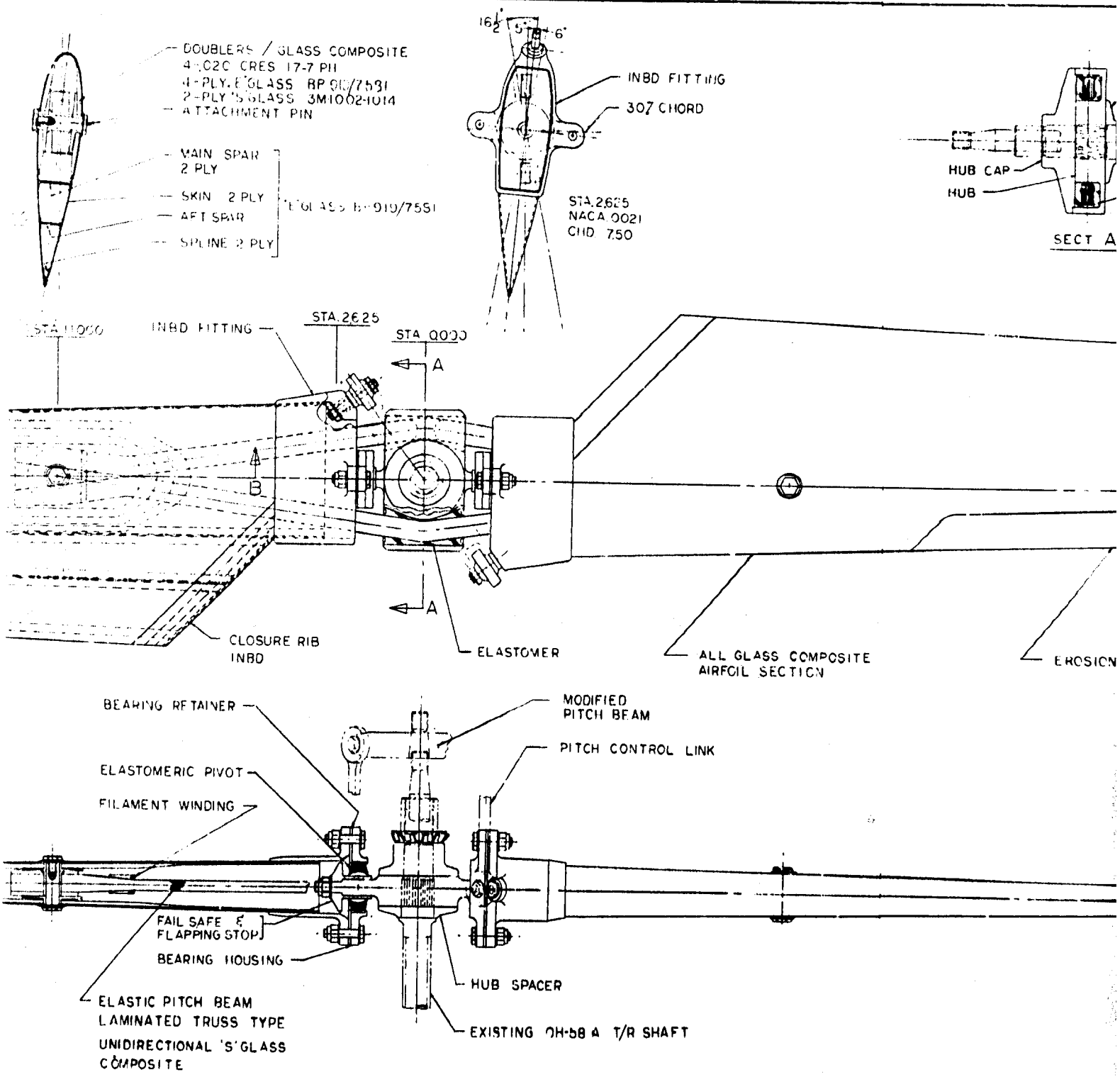

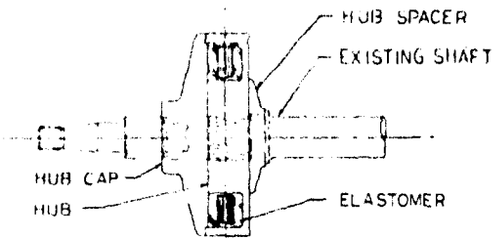

SECT A-A

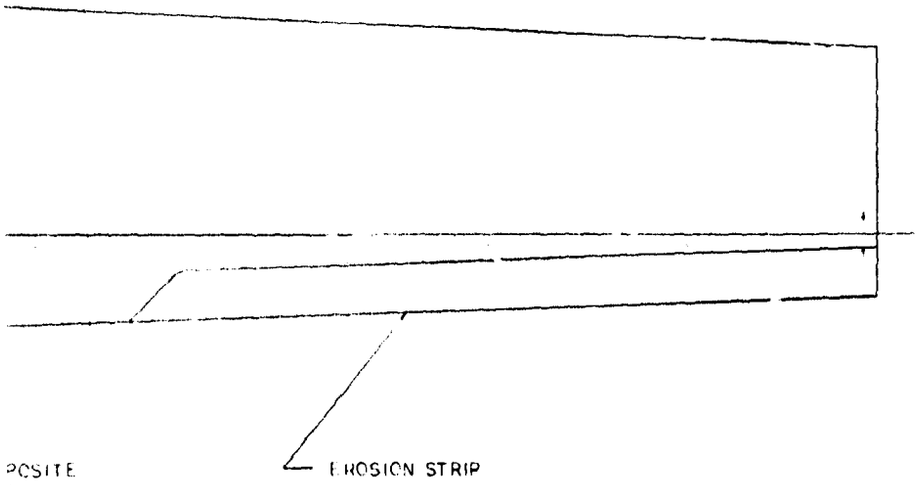

POSITE

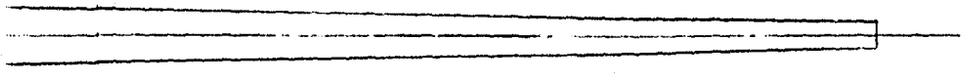

DESIGN DESCRIPTION

The basic details of the selected Elastic Pitch Beam tail rotor (EPBTR) designed for mounting on the OH-58A helicopter are shown in Figure 2. Pertinent physical dimensions and performance data for the current OH-58A tail rotor compared with those of the LOH Elastic Pitch Beam tail rotor design considered herein are as follows:

Item	Current Tail Rotor	EPBTR
Number of Blades	2	2
Diameter (ft)	5.17	5.17
Disc Area (sq ft)	20.97	20.97
Blade Chord (in.)	5.27	5.27 to 7.50
Rotor Solidity	.1078	.1309
Blade Area (sq ft)	2.26	2.75
Blade Airfoil (NACA)	0012.5	0012.5 to 0021
Delta Three (deg)	45	0
Direction of Rotation when Viewed from Left	Clockwise	Clockwise
Rotor Speed		
Power on, Maximum (rpm)	2627	2627
Power on, Minimum (rpm)	2575	2575
Power off, Maximum (rpm)	3050	3050
Power off, Minimum (rpm)	2256	2256
Maximum Power-On Torque (in.-lb)	1539	1539

Descriptions of the three major components making up the LOH Elastic Pitch Beam tail rotor assembly (Elastic Pitch Beam (EPB), airfoil section, and tail rotor hub) are presented in the following.

ELASTIC PITCH BEAM

The Elastic Pitch Beam portion of the tail rotor envisioned herein consists of a load-carrying structure that is continuous from the airfoil attachment points on each blade and passes through the torque transmitting hub at its center. This structure must carry the centrifugal force as well as the aerodynamic and dynamic inplane and out-of-plane bending moments imposed on it by the airfoil section while still retaining sufficient torsional flexibility to permit the full range of pitch change travel without introducing an appreciable increase in the required control load. As the basic helicopter performance characteristics such as rotor speed, tip speed, available power, and required thrust have already been established in the current tail rotor design, radical changes in the airfoil section required to accommodate the EPB cannot be tolerated if gains in performance are to be realized. Space must be provided within the airfoil section for the bolted connection between the airfoil section and the EPB, and for establishing the necessary clearance between the inboard end of the airfoil section and the EPB required for pitch change control. Therefore, the

geometry of the airfoil section and the Elastic Pitch Beam are closely interrelated, and care must be used in their selection. The Elastic Pitch Beam selected for use in the design of the LOH EPBTR is designated as the laminated truss-type EPB to distinguish it from other configurations studied in Reference 3. This EPB is a glass composite structure of 3M-1002-1014 unidirectional "S" glass configured to form a diamond-shaped truss that is symmetrical about its center at the hub and tapers outboard to form vertices at the point of airfoil section attachment. Reinforcing 17-7PH stainless steel doublers are provided at each end of the EPB to effect the transfer of the concentrated attachment bolt load into the glass composite structure of the EPB.

The diamond-shaped truss EPB configuration was selected for several reasons:

- The relatively low elastic torsional spring rate of the diamond-shaped truss minimizes the increase in the directional control system loads and thus eliminates, or minimizes, the necessity for installing load controlling centrifugal twisting moment counterweights.

- Centrifugal restoring or feathering moments acting at the outboard vertices of the EPB are minimized due to the small, compact cross section of the EPB.

- The reduction of the EPB's inplane stiffness with increasing torsional deflections about the pitch axis at the outboard vertices is eliminated due to the small, compact cross section of the truss.

The cross-sectional dimensions of each member making up the truss (.600 inch in width and .3125 inch in thickness), the separation of the truss members at the hub (3.10 inches), and the outboard intersection of the truss members (Station 11) were selected to minimize the out-of-plane bending stiffness and to maximize the inplane bending stiffness of the EPB without unduly increasing the thickness or planform of the airfoil section, and to minimize the torsional stiffness of the EPB.

The use of metallic reinforcing doublers at each end of the EPB, to aid in the transfer of concentrated bolt loads into the glass composite truss, was selected over other alternatives because:

- This type of attachment has been used with success in many helicopter main and tail rotor root-end designs.

- Due to its extended use in other designs, the capabilities of the attachment can be predicted with a high degree of confidence.

- The duties of the filament winding used just inboard of the attachment area to prevent local separation of the truss members being subjected to transverse shear and centrifugal forces are reduced since the doublers will aid the filament winding in preventing this separation.

- Should increased strength be required at this location to accommodate increased loading due to changes in helicopter mission requirements, additional doublers may be added to increase the bond area between the doublers and the glass composite laminae, and to increase the tension, shear, and bearing areas of the doublers at the attachment bolt hole without extensive modification to the tooling used in fabrication.

- Tooling required in the fabrication of this type of attachment is relatively simple and inexpensive when compared to other methods of attachment designs.

Materials used in the fabrication of the EPB were chosen because of their proven ability to withstand the anticipated flight loads and adverse environmental conditions, and also because of their availability and reasonable cost. For these reasons, 3M-1002-1014 "S" glass was chosen as the primary candidate material to be used in the fabrication of the EPB. Work completed under References 1 and 2 showed that the 3M-1002-1014 "S" glass has the required static and fatigue strength and sufficient stiffness, and that it is sufficiently compatible with the 17-7PH corrosion-resistant stainless steel used as reinforcing doublers.

Fabrication of the EPB will be accomplished through the use of a combination cavity form-bonding tool. Precut prepreg tapes of 3M-1002-1014 "S" glass and the 17-7PH stainless steel doublers will be layed up within the tool's cavity in their proper sequence until the appropriate laminae geometry is obtained. After an initial exposure to temperature, contoured cover plates will be closed down to limit stops and the final cure will be completed in an oven. Filament winding will be applied under uniform tensile load just inboard of the attachment areas at both ends of the EPB after the EPB is removed from the cavity form-bonding tool.

AIRFOIL SECTION

The airfoil section, selected from the Reference 3 design study for use on the LOH Elastic Pitch Beam tail rotor, is a monolithic glass composite structure designated as the "all-glass composite airfoil section". Basic features of this design, shown in Figure 2, include a leading-edge nose section, main and aft spars, wraparound upper and lower skins, trailing-edge spline, inboard fitting, and metallic reinforcing doublers in the bolt attachment areas. Inboard and outboard closure ribs, tip block, outboard metallic doublers, and erosion strip complete the airfoil section structure.

Outboard of the bolt attachment area the leading-edge nose section is built up from four plies of BP 919/7581 "E" glass, two of which are the wraparound skins, and two plies of 3M-1002-1014 "S" glass. Through the bolt attachment area and inboard of this location, two additional plies of BP 919/7581 are used to form the leading-edge nose section. Main and aft spars are four plies of BP 919/7581 "E" glass configured to form an "I" section having tapered flanges. BP 919/7581 "E" glass is also used to form the tapered cross section trailing-edge spline.

Four .020-inch-thick 17-7PH stainless steel doublers are interspersed between the glass composite laminae making the upper and lower surfaces of the leading-edge nose section in the area of the bolt attachment to transfer the loads developed in the airfoil section to the attachment bolt. Combination doubler-bushing fittings machined from 17-7PH stainless steel and located on the inner surfaces of the upper and lower portions of the leading-edge nose section are used as doublers to aid in distributing the airfoil section load into the attachment bolt, to align the doubler stack during fabrication, to establish the geometry required to accommodate the outer ends of the Elastic Pitch Beam, and to increase the bearing area of the four .020-inch-thick 17-7PH stainless steel doublers.

A 6061-T6 aluminum fitting bonded to the inboard end of the glass composite airfoil section provides a means for transforming linear pitch link travel into torisonal moments about the blade pitch axis for pitch angle control, and it provides a means for attaching the bearing housing and bearing retainer used in transferring airfoil section shear loads through the elastomeric pivot into the hub trunnions. If need be, the attachment lugs of the bearing housing may be reconfigured and extended to provide a means for attaching counterweights for regulating the effect of centrifugal restoring moment or for overcoming the torsional stiffness of the Elastic Pitch Beam.

Inboard and outboard closure ribs are provided for sealing off the aft portion of the airfoil section. The inboard and outboard ribs are fabricated from three staggered plies of BP 919/7581 "E" glass, with the inboard rib flanges being bonded over the wraparound skin and the outboard rib being molded monolithically to the inner surfaces of the wraparound skins. A phenolic tip block located at the outboard tip of the blade is used to close off the forward cavity formed by the leading-edge nose section and the main spar, and it provides a means for installing trim weights, when required, for fulfilling blade interchangeability requirements. The tip block is bonded and riveted to the airfoil section. Doublers made from 17-7PH stainless steel are provided at the outboard tip of the airfoil section to reinforce the riveted attachment.

A .060-inch-thick molded urethane erosion boot is bonded to the outboard leading-edge portion of the blade. Results of erosion testing of various candidate materials (Reference 2) indicate that urethane elastomers, as a group, showed much lower wear rates in sand than did metallic materials such as stainless steel, electroformed nickel, and titanium. During rain testing, however, the urethanes offered only limited protection against rain erosion. Should the urethane erosion boot be damaged by severe rain exposure, field replacement of this boot would be feasible at line level.

Fabrication of the airfoil section will be accomplished in three stages. During the first stage the main and aft spars, the two-ply wraparound skin, the inboard and outboard closure ribs, and the trailing edge spline will be layed up and cured as subassemblies. In the second stage, the doubler stacks, separated by a gage block, and the leading-edge nose section will

be layed up in a female mold, over an internal pressure diaphragm, and sandwiched between the precured wraparound skin and the pressure diaphragm. Main and aft spars and the trailing-edge spline will be placed in their proper position separated by two additional pressure diaphragms. The inboard fitting and the outboard closure rib will then be positioned and the female mold closed. After final cure, the pressure diaphragms will be removed, and the inboard closure rib will be bonded and the tip block bonded and riveted in place during the third stage.

HUB AND HUB AIRFOIL SECTION INTERFACE COMPONENTS

The hub selected for use on the LOH Elastic Pitch Beam tail rotor shown in Figure 2 is the two-bladed elastomeric hub investigated in the Reference 3 study program. This hub is compatible with the following design requirements:

- It provides a means for attaching the truss members of the Elastic Pitch Beam to the current OH-58A tail rotor shaft.
- It provides structure for resisting shear loads from the airfoil section and inplane and out-of-plane shear and bending moments from the Elastic Pitch Beam.
- It provides a means for transmitting blade thrust to the tail rotor shaft and tail rotor shaft torque to the blades.
- It is compatible with the desired inplane and out-of-plane natural frequencies required for rotor stability.
- It provides structure for resisting pitch control system loads.
- It eliminates the need for teeter bearings.
- It is of simple design to satisfy reliability, maintainability, and cost requirements.

The two-bladed elastomeric hub assembly consists of a 15-5PH stainless steel hub, a 2024-T4 aluminum hub cap, and a 15-5PH stainless steel hub spacer. Current OH-58A tail rotor shaft hardware such as the locking washer and attachment nut are used to complete this assembly.

The hub spacer and the hub cap are used to position the EPBTR hub on the current OH-58A tail rotor shaft such that the centerline of the EPBTR will be the same distance away from the pylon as is the current tail rotor blade. This is done to minimize changes in the control system and in the attachment hardware required to accommodate the LOH Elastic Pitch Beam tail rotor.

Basic features of the hub include two machined grooves, used for attaching the two truss members of the Elastic Pitch Beam; two trunnions, used for transferring airfoil section shear loads into the hub; and an internal spline located on the hub centerline and matching the current OH-58A tail rotor shaft spline, used for transmitting tail rotor shaft torque to the airfoil sections. The two grooves machined in the hub maintain the desired separation between the two Elastic Pitch Beam truss members and provide a means, through an elastomer, for obtaining a flexible attachment of the Elastic Pitch Beam to the hub. By the proper selection of the elastomer, its durometer, its free-edge configuration, and its physical dimensions, various inplane and out-of-plane stiffnesses may be obtained. Thus the ability to partially tailor the spring rates, or natural frequencies, of the tail rotor system by means of a simple material substitution is possible. Steady and vibratory out-of-plane bending stresses at the root end of the Elastic Pitch Beams would be minimal if the tail rotor blade could cone and flap freely about the flapping axis. Although complete flapping freedom cannot be achieved through this design, the out-of-plane bending stiffness of the Elastic Pitch Beam and the geometry and physical properties of the elastomer can be chosen to minimize the flapping restraint so that the out-of-plane bending stresses and hub movements may be reduced to tolerable levels. Dynamic stability requirements, however, dictate that the inplane stiffness of the Elastic Pitch Beam at the root and the stiffness of its attachment at the hub should be relatively high to preclude coincident out-of-plane and inplane natural frequencies. This goal is also obtainable by selecting the proper inplane bending stiffness of the Elastic Pitch Beam and by providing adequate lead-lag restraint through elastomer selection and configuration.

Trunnions, forming an integral part of the hub, are provided along the span axis of the tail rotor to resist shear forces caused by airloads and inertia loads acting on the airfoil section. These shear forces are transmitted from the airfoil section to the hub trunnions through the elastomeric pivot mounted in the 15-5PH stainless steel bearing housing attached to the inboard fitting of the airfoil section. The spherical portion of the elastomeric pivot permits flapping and lead-lag motion of the airfoil section with respect to the hub; the axial and rotational freedom between the bore of the bearing and the fail-safe - flapping stop bushing mounted on the hub trunnion allows the airfoil section to move outward to compensate for the stretching of the glass composite Elastic Pitch Beam when the rotor is brought up to speed, and it permits the airfoil section to be rotated through its pitch range.

The 15-5PH stainless steel fail-safe - flapping stop bushing serves several purposes in the LOH Elastic Pitch Beam tail rotor design. As mentioned above, it acts as a bearing surface to permit axial and rotational motion of the airfoil section relative to the hub while transferring the airfoil section shear loads into the hub. An antifriction coating such as Karon, a polymer composite, will be applied to the bearing surface of the bushing to permit the desired relative motions. The bushing also serves as a flapping stop to prevent the blades from contacting the pylon during

violent maneuvers or due to strikes with foreign objects. Flapping limits established for this design are set at approximately ± 8 degrees. At these extreme flapping angles, the bearing retainer will contact the flange of the fail-safe - flapping stop bushing to prevent further flapping excursions.

Should excessive spanwise motion of the airfoil sections occur during operation due to a partial Elastic Pitch Beam failure, stiffness degradation, or ballistic damage, the 15-5PH stainless steel bearing retainer would eventually come in contact with the flange portion of the fail-safe - flapping stop bushing, thus preventing the loss of an airfoil section and also limiting the amount of tail rotor unbalance that might develop. An antifriction coating will also be applied to the thrust face of the fail-safe - flapping stop bushing flange to limit the directional control forces that might develop during this situation to permit the helicopter to land safely. Adequate bond area is provided between the inboard fitting and the leading-edge nose section - main spar structure of the airfoil section to ensure the integrity of this secondary load path should a partial Elastic Pitch Beam failure occur.

Figure 3 is presented as an alternate design to the use of the elastomeric pivot for transferring the airfoil section shears into the hub trunnions. The design shown in Figure 3 uses a presently available, proven, sliding pivot bearing to provide the axial, rotational and pivot motion freedom required at this location. Minor changes to the inboard fitting, bearing retainer, bearing housing, fail-safe - flapping stop bushing, and hub trunnion would be required to accommodate this substitution.

The feasibility of designing four-bladed LOH Elastic Pitch Beam tail rotor systems using technology developed for the two-bladed OH-58A Elastic Pitch Beam tail rotors was explored in Reference 3. Figure 4 presents a conceptual design of a four-bladed Elastic Pitch Beam tail rotor that could be mounted on the current OH-58A tail rotor shaft and which would require only modifications to the directional control systems to accommodate four pitch links instead of two.

The transformation from a two-bladed system to a four-bladed system is accomplished by altering the hub to permit the incorporation of another set of a two-bladed rotor. Two additional grooves, offset along the tail rotor shaft and oriented 90 degrees to the initial set of grooves, are provided in the hub for containing the second two-bladed rotor set. As with the two-bladed elastomeric hubs previously described, the Elastic Pitch Beams of both rotor sets will be embedded in an elastomer. The configuration of the grooves and the elastomer can be selected to provide the desired inplane scissoring freedom between the two rotor sets while still maintaining sufficient inplane stiffness of each rotor assembly to preclude the occurrence of resonance problems.

An internal spline is provided in the hub to transfer torque from the current rotor shaft into the four rotor blades. Hub caps and hub spacers are keyed into the hubs of each configuration for structural continuity of the hub assembly.

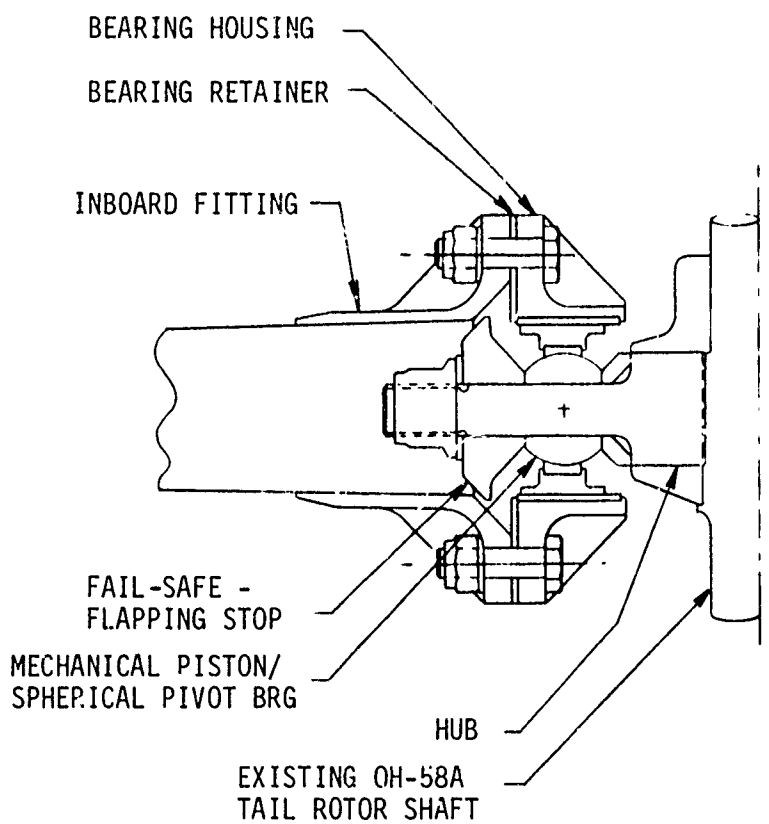

Figure 3. Alternate Design for Pitching and Flapping Axis.

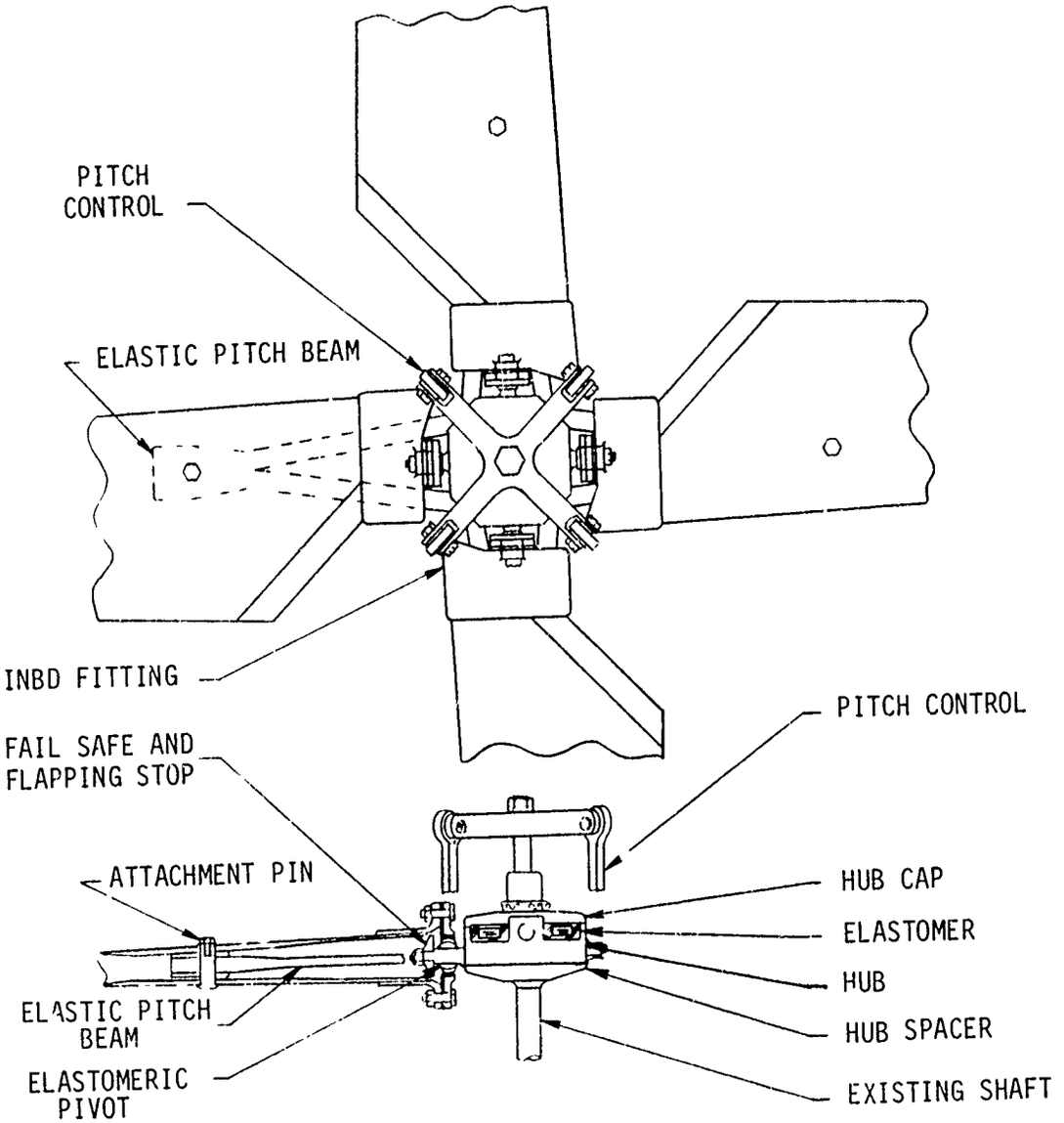

Figure 4. LOH Rotor Hub, Tail Rotor, 4-Bladed Elastomeric.

A redesign of the crosshead portion of the OH-58A tail rotor assembly will be required to provide collective pitch control for the four-bladed Elastic Pitch Beam tail rotor assembly shown in Figure 4. Modifications to the current pitch links will also be required due to the offset distance between the two sets of two-bladed Elastic Pitch Beam tail rotors wherein two sets of different length pitch links will be required to accomplish the desired pitch control for these rotor systems.

ROTOR ANALYSIS

The adequacy of the LOH Elastic Pitch Beam tail rotor design investigated herein was established by analytical procedures and methods. Anticipated aerodynamic performance of the airfoil section was evaluated in terms of tail rotor power required for a given rotor thrust; dynamic characteristics of the complete Elastic Pitch Beam tail rotor were obtained by dynamic analysis to establish the critical inplane and out-of-plane natural frequencies of the rotor system for the operational rotor speed range of the OH-58A; and the structural capability of this design was obtained through stress analysis performed at the critical sections of the rotor system.

POWER VERSUS THRUST

The power required at hover for various thrust levels was determined for both the current OH-58A tail rotor and the LOH Elastic Pitch Beam tail rotor. Power-thrust data, shown in Figure 5, was obtained at sea level and at an altitude of 4000 feet by using a hovering strip analysis called ZHSTRIP. This static thrust strip analysis considers the blade to be formed of several annuli, each functioning in a two-dimensional flow field. The resultant elemental lift and drag forces acting on the profile are resolved into thrust and torque components which are integrated for total thrust and torque. This strip analysis is based on the vortex theory modified by Goldstein corrections. Since the airfoil section of the LOH Elastic Pitch Beam tail rotor has both tapered thickness and tapered planform, combinations of two-dimensional airfoil data were used to represent this configuration.

The curves shown in Figure 5 indicate that the current OH-58A tail rotor and the LOH Elastic Pitch Beam tail rotor have similar power requirements at the lower thrust levels. At the higher thrust levels, however, the LOH EPBTR requires less power for a given amount of thrust than does the current OH-58A tail rotor. These differences are largely due to the higher solidity (larger effective chord) of the EPBTR, so at the higher thrust levels, less blade pitch is required to generate a given thrust level. It is therefore concluded that by using the EPBTR, more power will be available in the higher thrust regions where more margin is required for maneuvers.

NATURAL FREQUENCIES

Inplane and out-of-plane natural frequencies were calculated for the LOH Elastic Pitch Beam tail rotor, and the results are presented in Figure 6. These analyses were made to ensure that the rotor's natural frequencies were not coincident with the rotor's operational frequencies and that there is sufficient separation between the inplane and out-of-plane natural frequencies to preclude the occurrence of instability problems due to inplane and out-of-plane coupling.

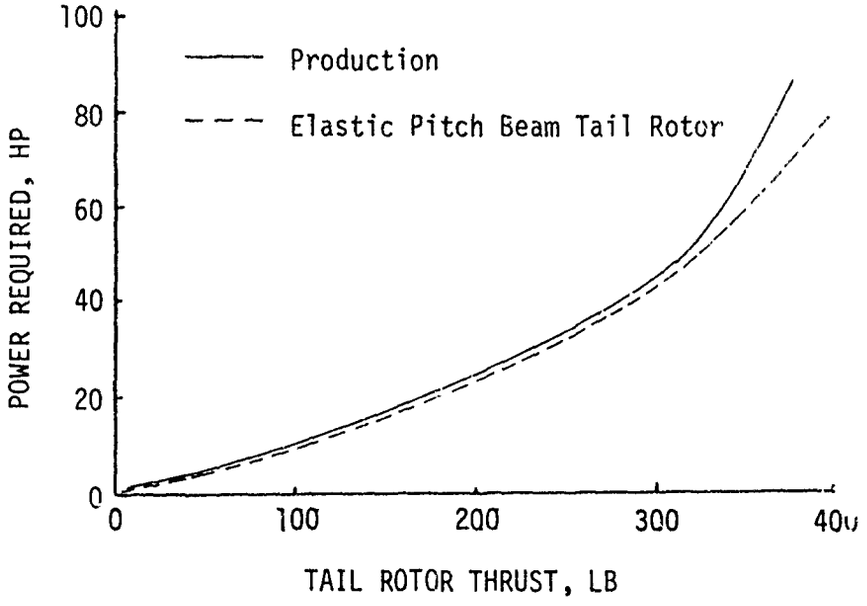

(a) Sea Level

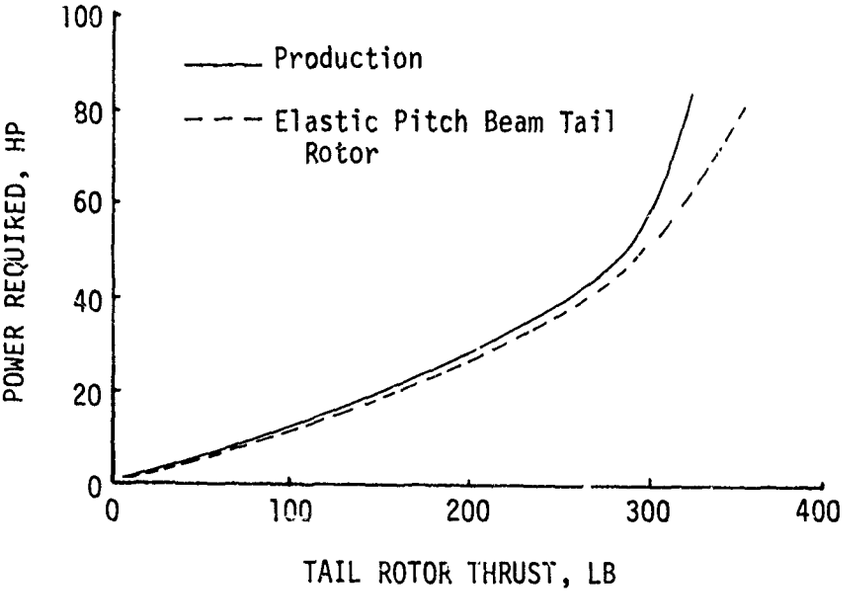

(b) 4000-Foot Altitude

Figure 5. Power Versus Thrust Curves for OH-58A Production and Elastic Pitch Beam Tail Rotors.

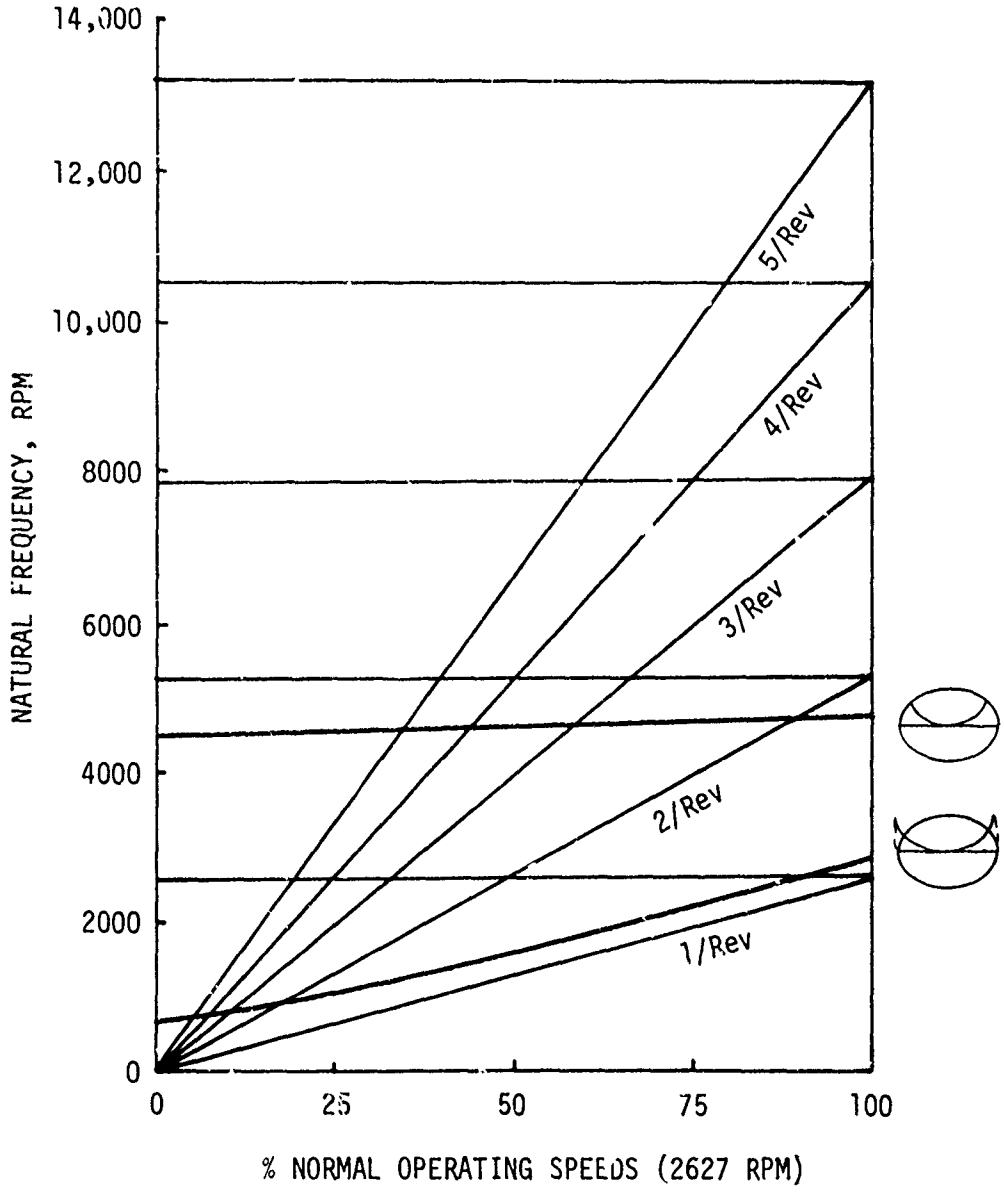

Figure 6. Frequency Plot for OH-58A Elastic Pitch Beam Tail Rotor.

Where possible, established analytical techniques and available computer programs were utilized to obtain the desired natural frequencies. In general, the natural frequencies and mode shapes were calculated using an iteration procedure called the "Modified Stodola Method", wherein the mode shape is initially defined by a set of trail deflections. New deflections which would result from the inertial and operating loads associated with the trail deflections are calculated. Trail deflections are modified until the trail deflections and the calculated deflections coincide within iteration tolerance. Due to the uniqueness of the Elastic Pitch Beam concept, modifications to the standard computer programs were required to establish the equivalent inplane and out-of-plane bending stiffnesses of the overlapping beam configuration characteristic of the Elastic Pitch Beam concept investigated herein. For practical purposes, it was assumed that the effects of coincident natural frequency and operational frequency at frequencies higher that 5/rev are ineffectual in creating serious dynamic problems associated with resonance, as structural and air dampening are relatively high at these frequencies. Basic section properties for the LOH Elastic Pitch Beam tail rotor used in the dynamic analyses, and in the stress analyses to follow, are shown in Figures 7 through 11. As shown in Figure 6, the first cantilever inplane mode natural frequency for the LOH Elastic Pitch Beam tail rotor is approximately 1.8/rev, and the first cantilever out-of-plane mode natural frequency is approximately 1.1/rev Higher natural frequencies for both the inplane and out-of-plane cantilever bending modes are above 5/rev and are therefore considered to be ineffectual in creating serious resonant problems.

STRUCTURAL ANALYSIS

The critical areas of the LOH Elastic Pitch Beam tail rotor shown in Figure 2 are considered to be:

- The outboard Elastic Pitch Beam - airfoil section attachment area.
- The root end of the Elastic Pitch Beam as it emerges from the hub.
- The airfoil section at the point of maximum combined stress.
- The hub trunnion on which the elastomeric pivot is mounted.
- The fail-safe provisions incorporated in the hub-inboard airfoil section design.
- The current production OH-58A shaft on which the EPBTR is mounted.

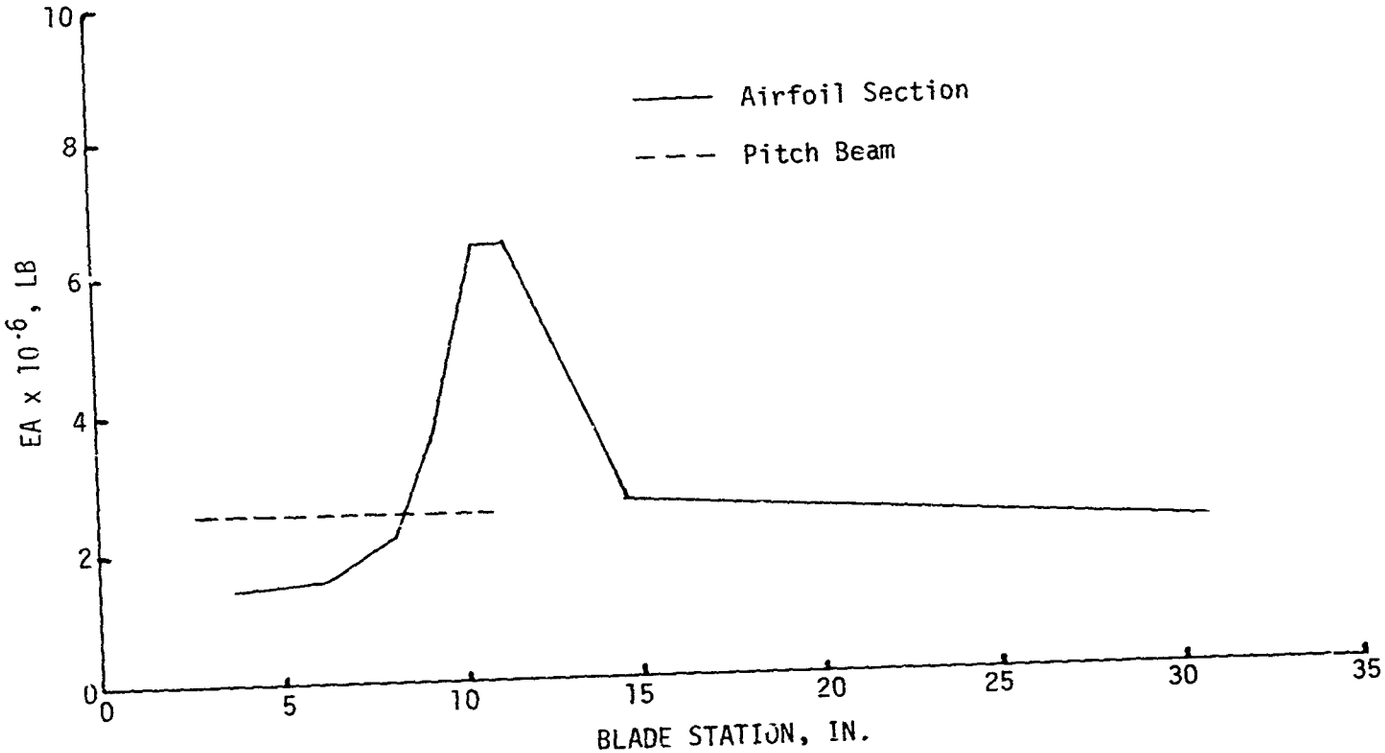

Figure 7. Axial Stiffness Distribution for OH-58A Elastic Pitch Beam Tail Rotor.

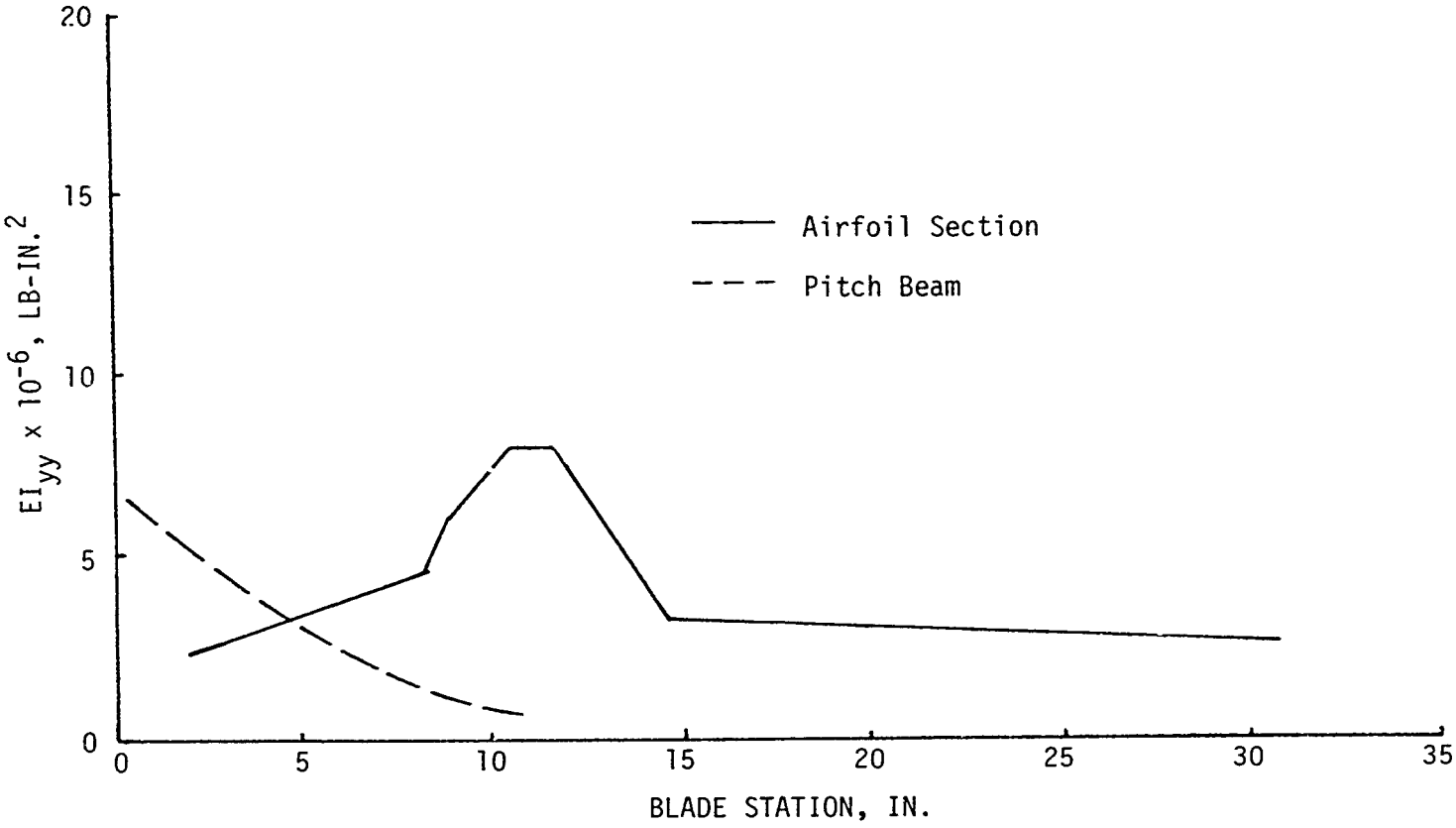

Figure 8. Edgewise Stiffness Distribution for OH-58A Elastic Pitch Beam Tail Rotor.

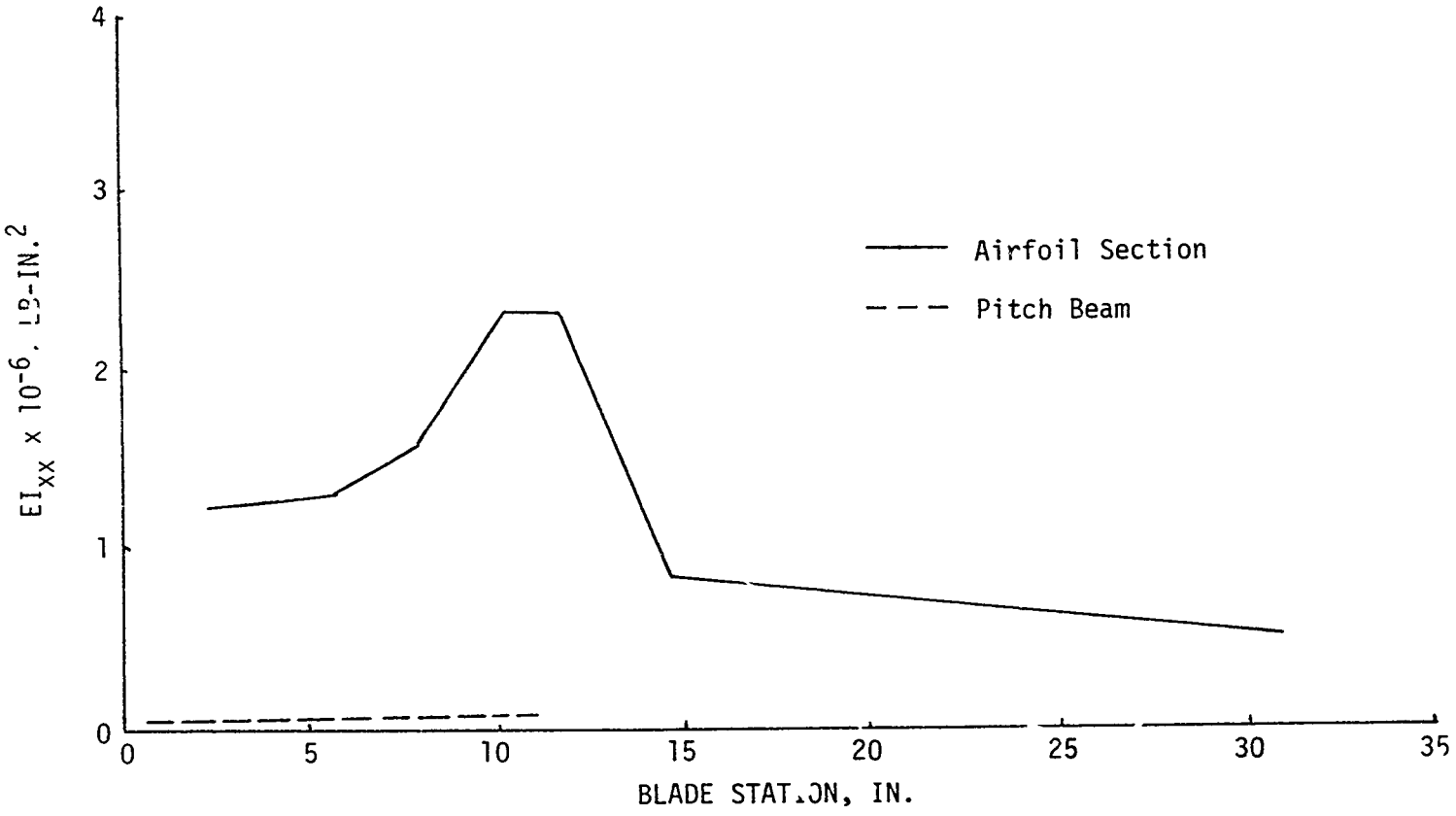

Figure 9. Flatwise Stiffness Distribution for OH-58A Elastic Pitch Beam Tail Rotor.

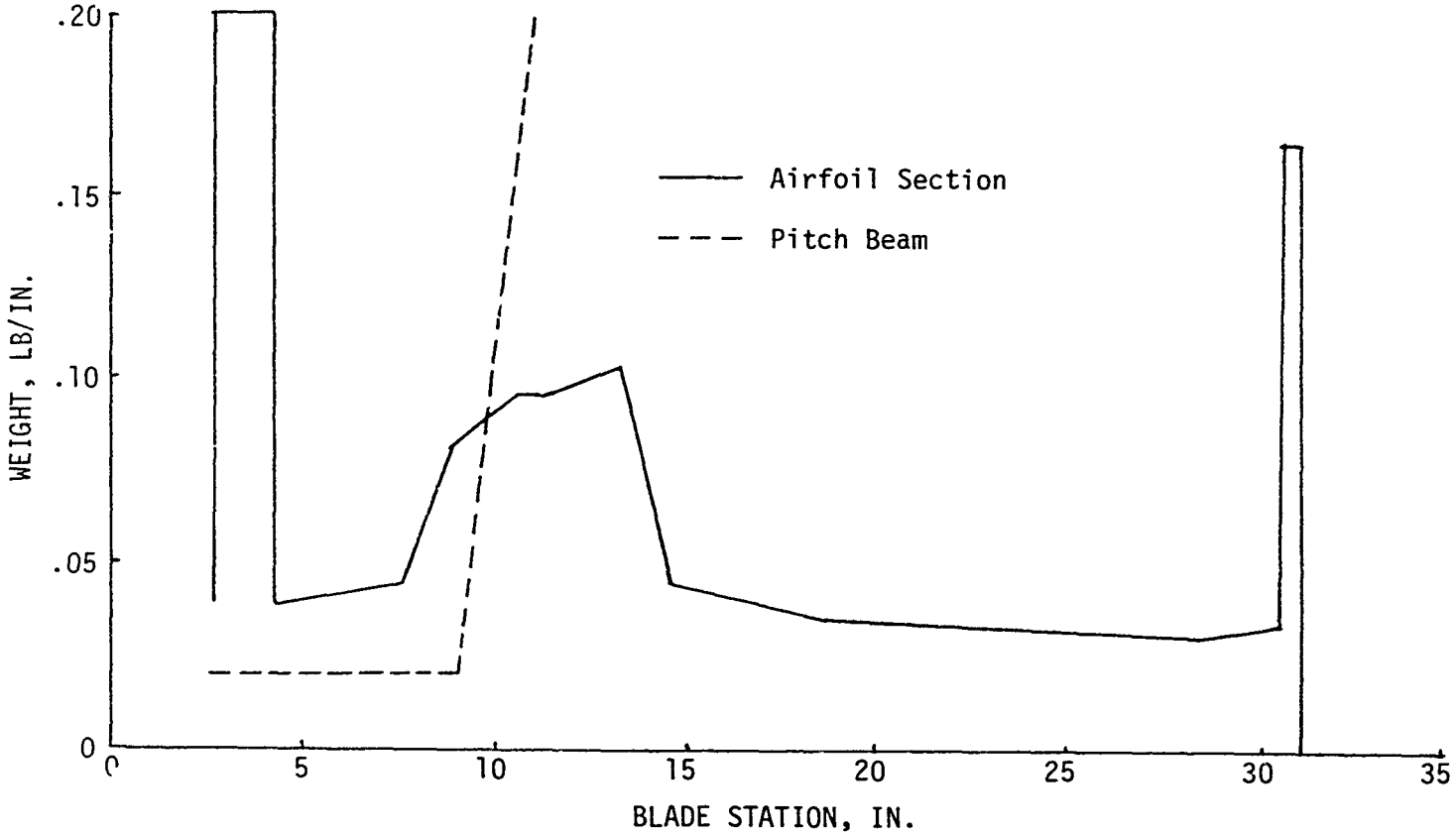

Figure 10. Spanwise Weight Distribution for OH-58A Elastic Pitch Beam Tail Rotor.

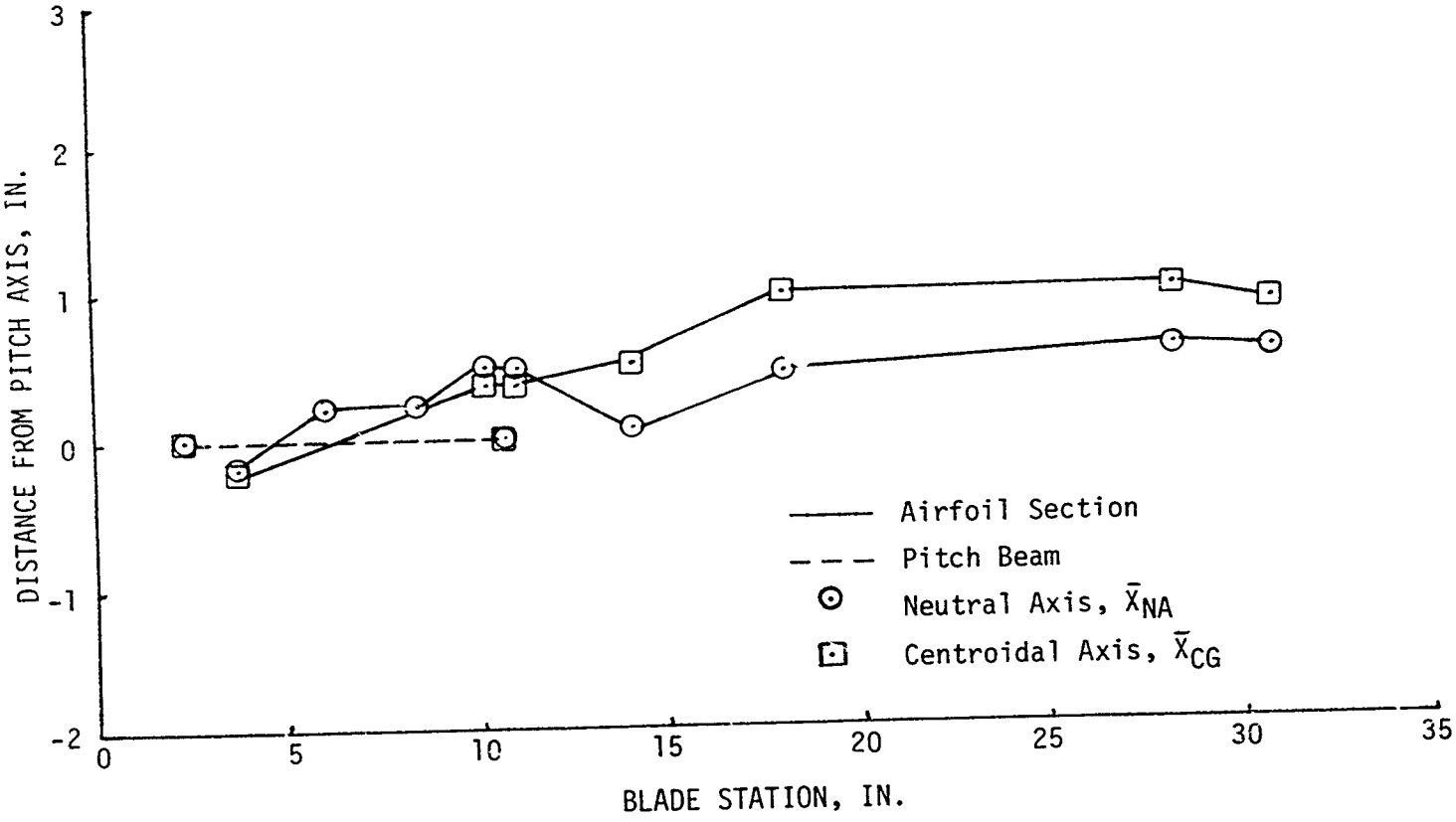

Figure 11. Spanwise Neutral Axis and Centroidal Axis Distributions for OH-58A Elastic Pitch Beam Tail Rotor.

Elastic Pitch Beam - Airfoil Section Attachment

The principal load acting on the EPB - airfoil section attachment area is the centrifugal force of the airfoil section. Reactions due to inplane and out-of-plane steady and vibratory bending moments acting at this location are secondary in magnitude and are therefore neglected. Figure 12 shows that the limit centrifugal force acting at the attachment area is 5700 lb. The ultimate centrifugal force would then be 1.5 (5700) = 8550 lb. To ensure that the attachment area has a potential for withstanding higher centrifugal force loadings due to possible airfoil section design changes that would result in an increase in airfoil section weight and thus centrifugal force, the design ultimate centrifugal force load was increased to 15,000 pounds. The attachment areas of the Elastic Pitch Beam and the airfoil sections were therefore designed to withstand an ultimate axial load, P_u = 15,000 lb.

1. Elastic Pitch Beam Outboard Attachment Area

Figure 13 presents the details of the Elastic Pitch Beam attachment area. Axial loads coming into the EPB from the airfoil section are transferred from the attachment bolts into nine .020-inch-thick 17-7PH stainless steel doublers and thence into the 3M-1002-1014 "S" glass composite laminates forming the individual truss members of the EPB. The thickness of the glass composite laminates lying between each of the stainless steel doublers varies such that the outer laminates are thinner than those in the center. In analyzing this type of joint, it was assumed that the load in each doubler is proportional to the average load-carrying capabilities of the glass composite laminates lying on either side of them such that the inner doublers would be carrying a higher percentage of the total load than would the outer ones. It is also assumed that the 6061-T6 aluminum cheek plates 'A) lying on either side of the outer stainless steel doublers are not structurally effective in transferring load from the bolt to the stainless steel doublers and are therefore neglected in the analysis. Table 1 lists the thicknesses of each glass composite laminate, the axial load (P_L) taken by each laminate, the distribution of bond area for each doubler, the distribution of bond area for each laminate, the bond stress for each doubler-laminate interface, and the load taken by each doubler. Doubler and laminate designations are as shown in Figure 13.

Using the unit interface bond stress data from Table 1, the maximum bond stress between the doublers and the glass composite laminate for an axially applied ultimate load of 15,000 pounds is found to be:

$$f_{ibu} = .0518\ P_u$$

$$f_{ibu} = .0518\ (15{,}000)$$

$$f_{ibu} = 777 \text{ psi}$$

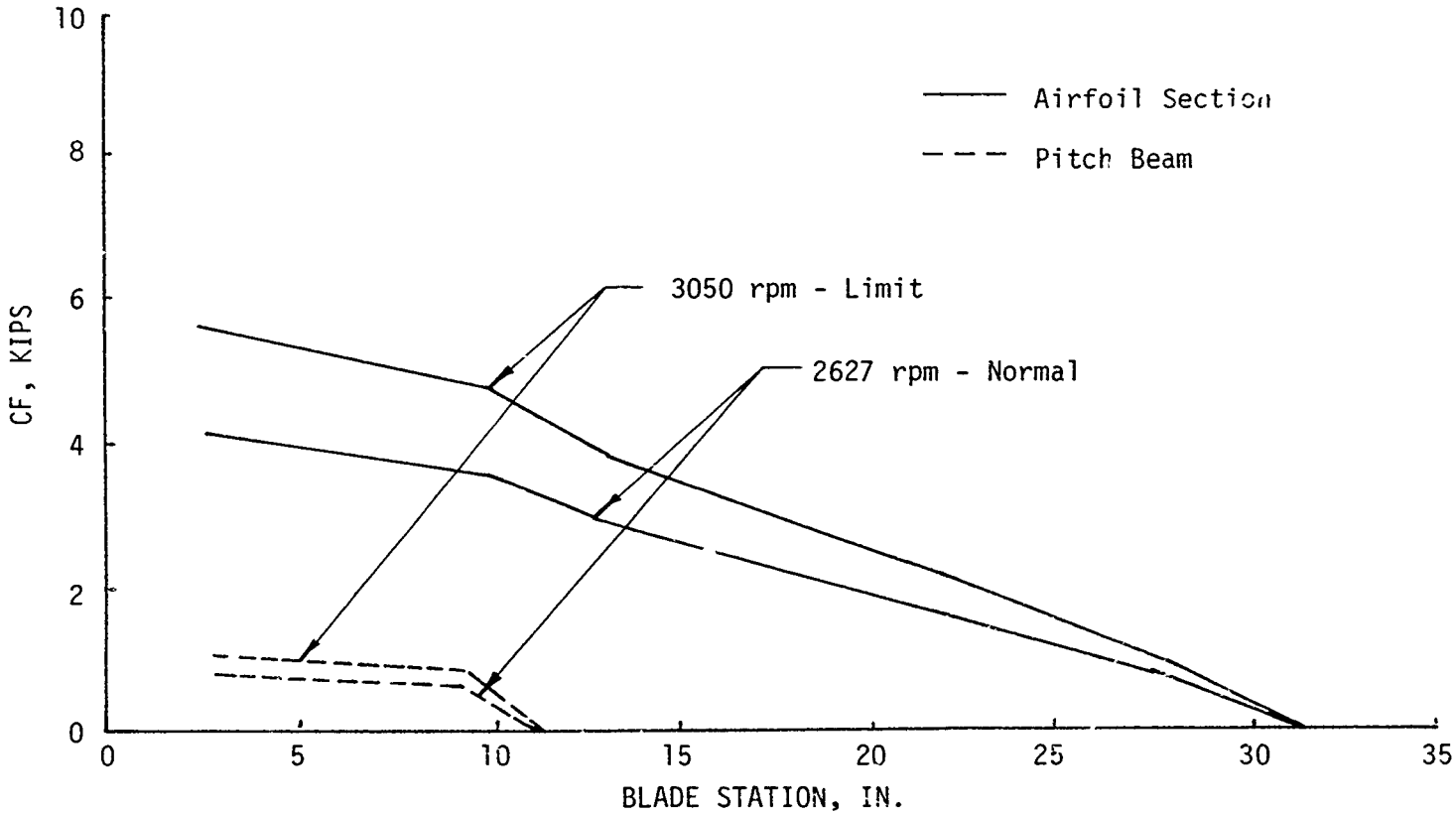

Figure 12. Centrifugal Force Distribution for OH-58A Elastic Pitch Beam Tail Rotor.

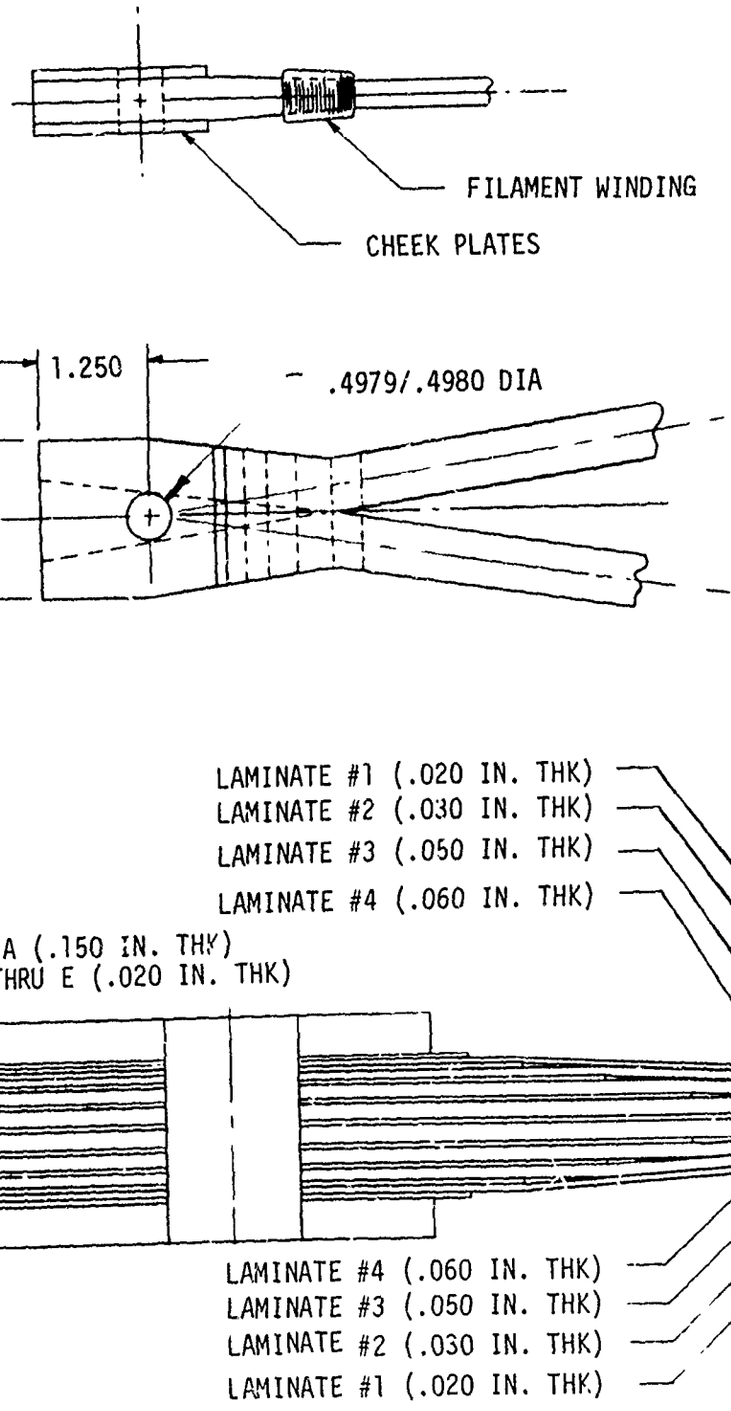

Figure 13. Elastic Pitch Beam Attachment Area, Sta 11.00, OH-58A.

TABLE I. OUTBOARD ELASTIC PITCH BEAM ATTACHMENT AREA UNIT LOADS AND UNIT BOND STRESSES

Doubler Letter (Figure 13)	Laminate Number (Figure 13)	Laminate Thickness t_L (in.)	Laminate Load P_L (lb)	Doubler Bond Area A_{bd} ($in.^2$)	Laminate Bond Area A_{bL} ($in.^2$)	Interface[a] Bond Stress f_{ib} (psi)	Doubler Load P_d (lb)
B				1.190			.0312 P
	1	.020	.0625 P		2.502	.0250 P	
C				2.625			.0781 P
	2	.030	.0938 P		2.808	.0334 P	
D				2.992			.1250 P
	3	.050	.1562 P		3.186	.0490 P	
E				3.379			.1719 P
	4	.060	.1875 P		3.622	.0518 P	
F				3.664			.1876 P
	5	.060	.1875 P		3.622	.0518 P	
E				3.379			.1719 P
	6	.050	.1562 P		3.186	.0490 P	
D				2.992			.1250 P
	7	.030	.0938 P		2.808	.0334 P	
C				2.625			.0781 P
	8	.020	.0625 P		2.502	.0250 P	
B				1.190			.0312 P
Totals		.320	P	24.236	24.236		P

(a) Interface bond stress, $f_{ib} = P_L/A_{bL}$

Lap shear tests between 17-7PH stainless steel and 3M-1002-1014 "S" glass composite laminates bonded with B.F. Goodrich 717 (Plastilock) adhesive show that the ultimate bond strength of this combination is from 3000 to 4000 psi. Conservatively using an ultimate bond strength of 1000 psi, the margin of safety for adhesive bond between the stainless steel doublers and the glass composite laminates is found to be

$$MS_{su} = \frac{1000}{.777} - 1$$

$$MS_{su} = \underline{\underline{.29}}$$

Bond stresses for the remaining interfaces and their respective margin of safety are shown in Table 2.

The maximum ultimate laminate tensile load shown in Table 1 was found to be

$$P_{Lu} = .1875\ P_u$$

$$\text{for } P_u = 15{,}000 \text{ lb}$$

$$P_{Lu} = .1875\ (15{,}000)$$

$$P_{Lu} = 2812.5 \text{ lb}$$

The ultimate tensile stress in this laminate is then

$$f_{tu} = \frac{P_{Lu}}{A_L}$$

Using the width of the laminates as 1.2 inches (twice the width of an individual EPB truss member), this can also be expressed as

$$f_{tu} = \frac{P_{Lu}}{1.2\ t_L}$$

Therefore, for the highest loaded laminate,

$$f_{tu} = \frac{2812.5}{1.2(.06)}$$

$$f_{tu} = 39{,}062 \text{ psi}$$

As the ultimate strength for the 3M-1002-1014 "S" glass composite is 220,000 psi, the margin of safety is then

$$MS_{tu} = \frac{220{,}000}{39{,}062} - 1$$

$$MS_{tu} = \underline{\underline{4.63}}$$

TABLE 2. OUTBOARD ELASTIC PITCH BEAM ATTACHMENT AREA ULTIMATE STRESSES AND MARGINS OF SAFETY FOR ULTIMATE CENTRIFUGAL LOAD OF 15,000 POUNDS

Doubler Letter (Figure 13)	Laminate Number (Figure 13)	Ultimate Interface Bond Stress		Ultimate Laminate Tensile Stress		Ultimate Doubler Tensile Stress		Ultimate Doubler Shear Stress		Ultimate Doubler Bearing Stress	
		f_{ibu} (psi)	MS_{su}	f_{tu} (psi)	MS_{tu}	f_{tu} (psi)	MS_{tu}	f_{su} (psi)	MS_{su}	f_{bru} (psi)	MS_{bru}
B						18,720	8.46	11,700	8.83	46,800	6.56
	1	375	1.67	39,062	4.63						
C						46,860	3.78	29,288	2.93	117,150	2.02
	2	501	1.00								
D						75,000	1.36	46,875	1.45	187,500	.89
	3	735	.36								
E						103,140	.72	64,462	.78	257,850	.37
	4	777	.29								
F						112,560	.57	70,353	.63	281,400	.26
	5	777	.29								
E						103,140	.72	64,462	.78	257,850	.37
	6	735	.36								
D						75,000	1.36	46,875	1.45	187,500	.89
	7	501	1.00								
C						46,860	3.78	29,288	2.93	117,150	2.02
	8	375	1.67	39,062	4.63						
B						18,720	8.46	11,700	8.83	46,800	6.56

As indicated in Table 2, the ultimate tensile stresses and their respective margins of safety are the same for each laminate.

Ultimate tensile, shear, and bearing stresses in the doublers are critical at the attachment bolt hole. From Table 1, the highest loaded doubler is doubler "F". The ultimate load applied to this doubler is

$$P_{du} = .1875P_u$$

$$P_{du} = .1875(15{,}000)$$

$$P_{du} = 2814 \text{ lb}$$

The net tensile area at the bolt hole is

$$A_t = (1.75 - .50)(.020) = .025 \text{ in.}^2$$

and the resulting ultimate tensile stress in the doubler at this location is:

$$f_{tu} = \frac{P_{du}}{A_t}$$

$$f_{tu} = \frac{2814}{.025}$$

$$f_{tu} = 112{,}560 \text{ psi}$$

The ultimate tensile strength of the 17-7PH stainless steel doublers is 177,000 psi (from Reference 4). The margin of safety in tension for the maximum loaded doubler is then:

$$MS_{tu} = \frac{177{,}000}{112{,}560} - 1$$

$$MS_{tu} = \underline{\underline{.57}}$$

Ultimate tensile stresses and margins of safety for the other doublers are shown in Table 2.

From Figure 13, the shear area for each doubler is found to be

$$A_s = 2(1.25 - .25)(.020)$$

$$A_s = .040 \text{ in.}^2$$

and the ultimate shear stress in doubler "F" is then

$$f_{su} = \frac{P_{du}}{A_s}$$

$$f_{su} = \frac{2814}{.040}$$

$$f_{su} = 70{,}350 \text{ psi}$$

From Reference 4, the ultimate shear strength for 17-7PH stainless steel is 115,000 psi. The ultimate margin of safety for doubler shear is then

$$MS_{su} = \frac{115,000}{70,350} - 1$$

$$MS_{su} = \underline{\underline{.63}}$$

The doubler bearing area at the bolt hole is found to be

$$A_{br} = (.50)(.020)$$

$$A_{br} = .010 \text{ in.}^2$$

and the ultimate bearing stress in doubler "F" is determined by

$$f_{bru} = \frac{P_{du}}{A_{br}}$$

$$f_{bru} = \frac{2814}{.010}$$

$$f_{bru} = 281,400 \text{ psi}$$

As the ultimate bearing strength for 17-7PH stainless steel obtained from Reference 4 is 354,000 psi, the margin of safety for ultimate bearing is

$$MS_{bru} = \frac{354,000}{281,400} - 1$$

$$MS_{bru} = \underline{\underline{.26}}$$

As noted by a review of Table 2, the outboard attachment area of the Elastic Pitch Beam is most critical either in the interface bond between the stainless steel doubler "F" and the glass composite laminates on either side or in the bearing on the doubler "F" at the attachment bolt hole. If additional strength is required in the Elastic Pitch Beam at this location, additional doublers may be added to reduce the bond stress, and the thickness of the doublers may be increased to reduce the bearing stress.

2. Airfoil Section Attachment Area

The attachment area of the airfoil section is conservatively designed for an ultimate centrifugal force equal to 15,000 pounds. Loads originating in the glass composite airfoil section are transferred into the attachment bolt by the use of eight .020-inch-thick 17-7PH stainless steel doublers and two doubler-bushing fittings that are molded monolithically within the glass composite structure. As shown in Figure 14, the leading-edge spar portion of the glass composite airfoil section is divided into five laminates separated by the doublers. The outer laminate, laminate number 1, consists of two plies of BP 919/7581 forming the wraparound skins; the second laminate, laminate number 2, is two plies of 3M-1002-1014 "S" glass used for stiffening the leading-edge spar; the third laminate, laminate number 3, is two plies of BP 919/7581 glass composite; and the fourth and fifth laminates, laminate numbers 4 and 5, are one ply each of BP 919/7581 glass composite.

It is assumed in this stress analysis that the loads in each of the laminates are proportional to the unit axial stiffnesses of each laminate (Et) and that the load in each doubler is the average of the loads carried by the laminates lying on either side of the doubler. It is further conservatively assumed that the effective width of the laminates is equal to the mean width of the doublers lying on either side of them.

Table 3 presents the doubler identification letter, the laminate identification number, the equivalent laminate thickness using BP 919/7581 glass composite as the base material, the load in each laminate, the total doubler bond area, the average bond stress between the laminates and the doublers, and the load in each doubler.

The detailed stress analysis for the airfoil section attachment area was performed in a manner similar to that previously shown for the outboard attachment area of the Elastic Pitch Beam, and a summary of the results is shown in Table 4. High margins of safety were found for all locations analyzed with the exception of those determined for the inner laminates. As the assumption concerning the effective width of the laminates is quite conservative, the actual stress levels in these laminates are not as severe as indicated and good performance in this area is anticipated.

3. Attachment Bolt

The 3/8-inch-diameter attachment bolt will have a low-profile head and nut. Provisions will be made in the threaded portion of the bolt so that a tab lock washer may be used to lock the nut to the bolt. The material for both bolt and nut will be alloy steel having an ultimate tensile strength of 160,000 psi, an ultimate shear strength of 95,000 psi, and an ultimate bearing strength of 219,000 psi.

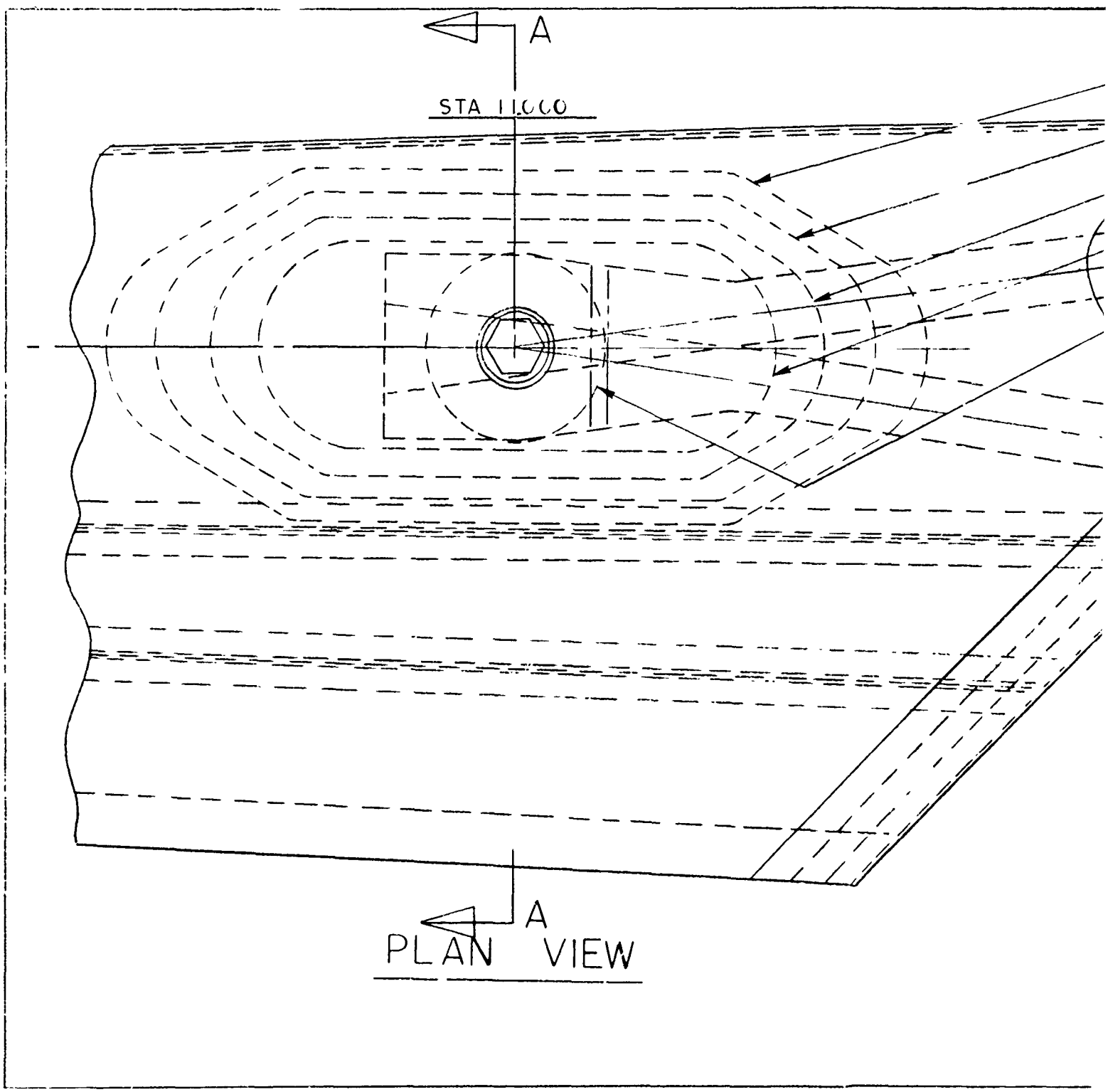

Figure 14. Airfoil Section Attachment Area, Station 11.00, OH-58A.

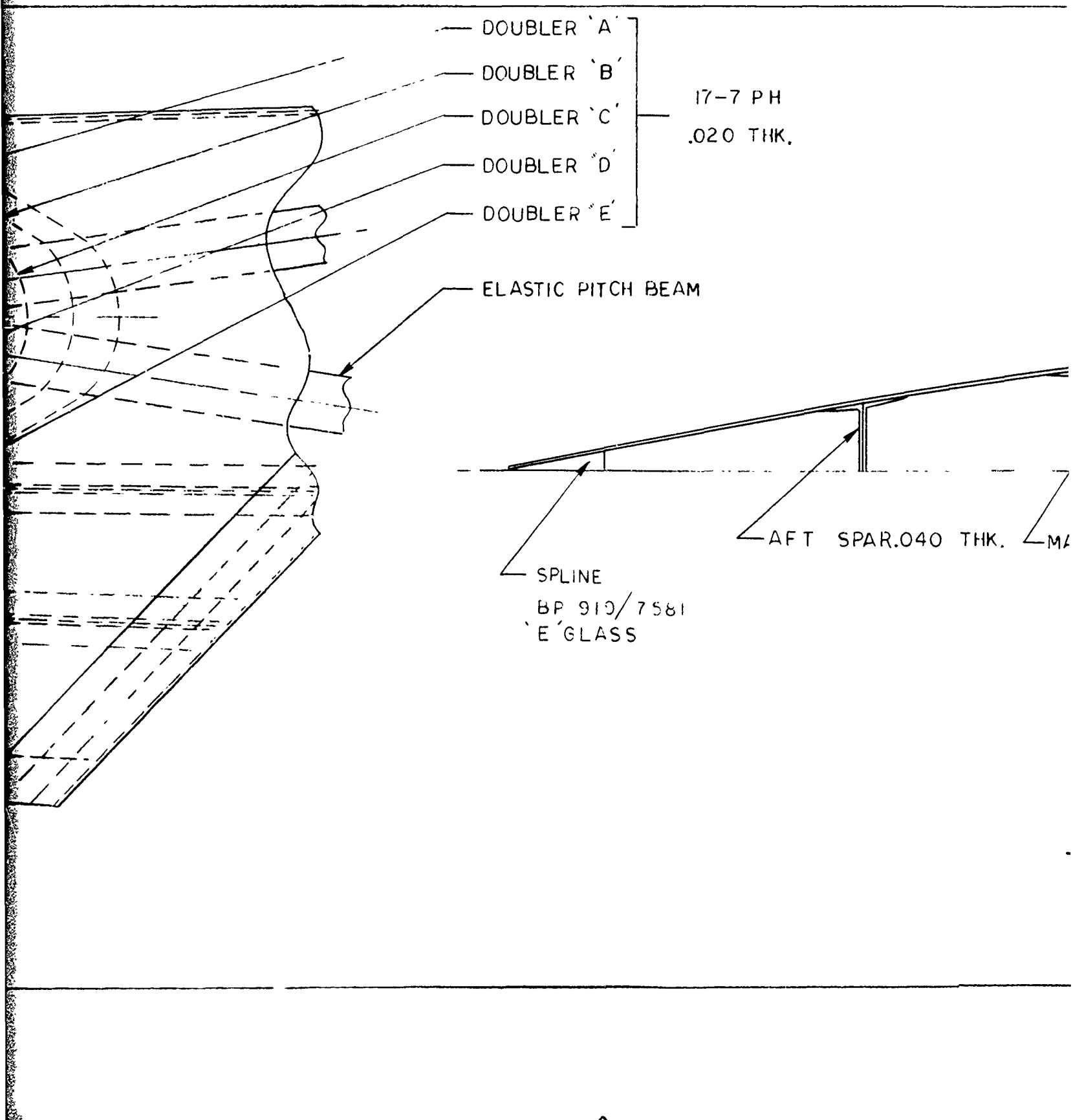
DOUBLER 'A'
DOUBLER 'B'
DOUBLER 'C'
DOUBLER 'D'
DOUBLER 'E'
17-7 PH
.020 THK.
ELASTIC PITCH BEAM
AFT SPAR.040 THK.
SPLINE
BP 910/7581
'E' GLASS

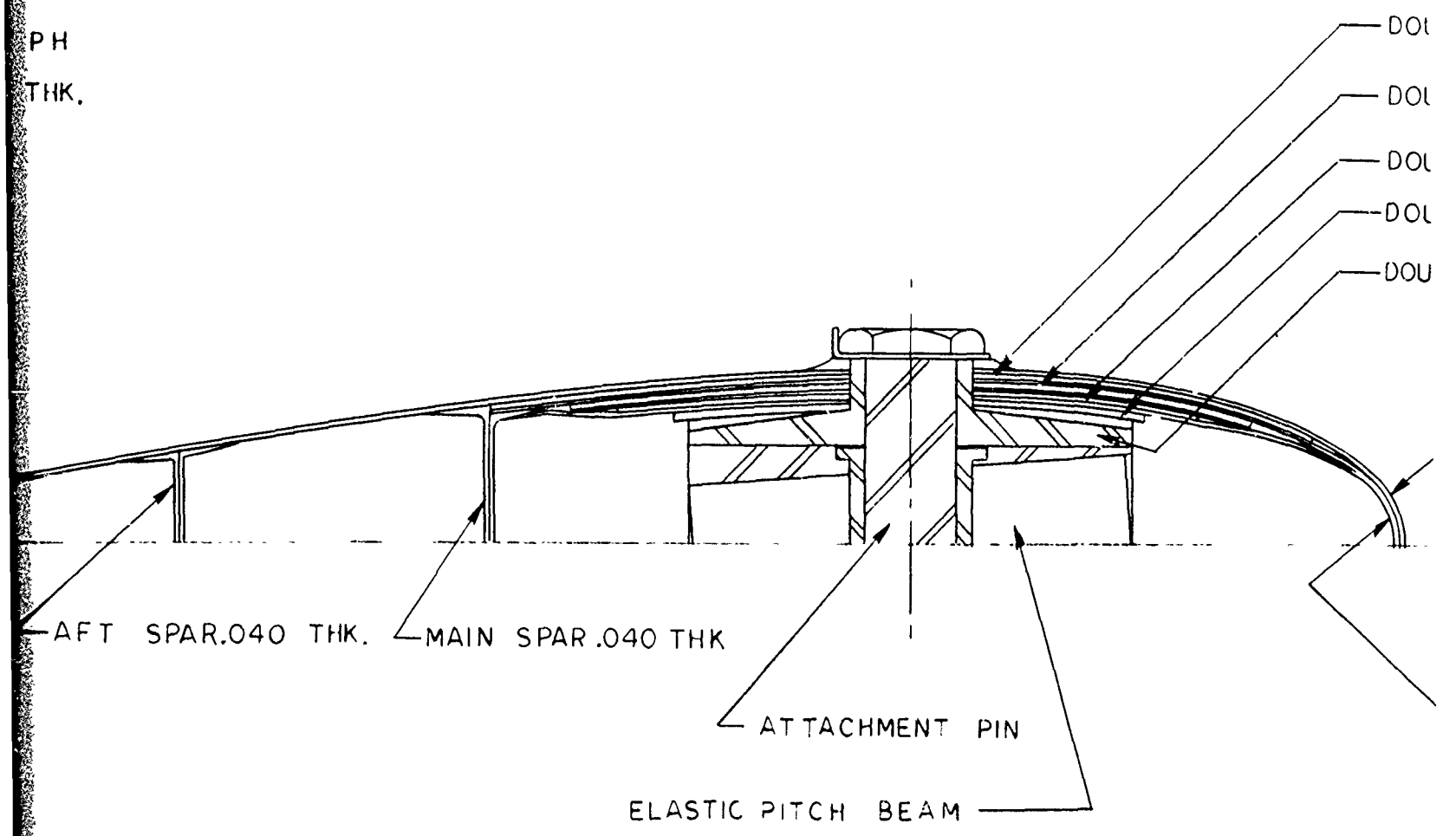

SECT A-A

ROTATED 90°

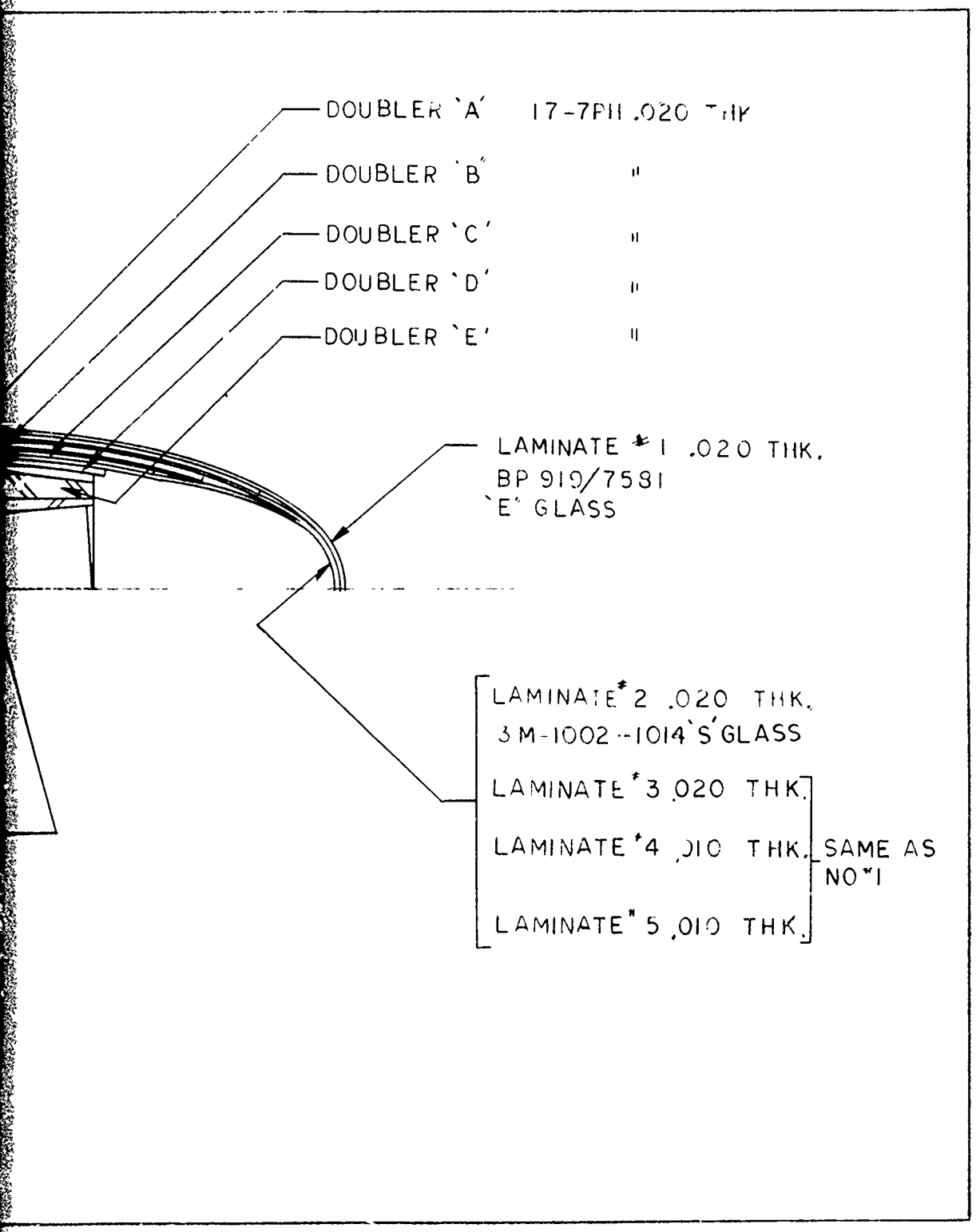
DOUBLER 'A' 17-7PH .020 THK
DOUBLER 'B' "
DOUBLER 'C' "
DOUBLER 'D' "
DOUBLER 'E' "
LAMINATE #1 .020 THK.
BP 919/7581
'E' GLASS
LAMINATE #2 .020 THK.
3M-1002-1014 'S' GLASS
LAMINATE #3 .020 THK.
LAMINATE #4 .010 THK.
SAME AS NO #1
LAMINATE #5 .010 THK.

TABLE 3. AIRFOIL SECTION ATTACHMENT AREA UNIT AND BOND STRESSES

Doubler[a] Letter (Figure 14)	Laminate[b] Number (Figure 14)	Equivalent Laminate Thickness t_L (in.)	Laminate Load P_L (lb)	Doubler Bond Area A_{bd} (in.^{2})	Laminate Bond Area A_{bl} (in.^{2})	Interface Bond Stress f_{il} (psi)	Doubler Load P_d (lb)
	1	.020	.0935 P		21.907	.0043 P	
A				43.814			.2033 P
	2	.047	.2196 P		38.802	.0056 P	
B				33.790			.1566 P
	3	.020	.0935 P		29.024	.0032 P	
C				24.258			.0701 P
	4	.010	.0467 P		19.641	.0024 P	
D				15.024			.0467 P
	5	.010	.0467 P		9.475	.0049 P	
E				1.963			.0233 P
E				1.963			.0233 P
	5	.010	.0467 P		9.475	.0049 P	
D				15.024			.0467 P
	4	.010	.0467 P		19.641	.0024 P	
C				24.258			.0701 P
	3	.020	.0935 P		29.024	.0032 P	
B				33.790			.1566 P
	2	.047	.2196 P		38.802	.0056 P	
A				43.814			.2033 P
	1	.020	.0935 P		21.907	.0043 P	
Totals		.214	P	237.698	237.698		P

(a) Doublers A, B, C & D are .020 inch thick 17-7 PH stainless steel. Doubler E, machined from 17-7 PH stainless steel, has an average flange thickness of .040 inch.

(b) Laminates 1 & 3 = 2-ply BP 919/7581, Laminate 2 = 2-ply 3M-1002-1014 "S" Glass, Laminates 4 & 5 = 1-ply BP 919/7581.

TABLE 4. AIRFOIL SECTION ATTACHMENT AREA ULTIMATE STRESSES AND MARGINS OF SAFETY FOR AN ULTIMATE CENTRIFUGAL LOAD OF 15,000 POUNDS

Doubler Letter (Figure 14)	Laminate Number (Figure 14)	Ultimate Interface Bond Stress		Ultimate Laminate Tensile Stress		Ultimate Doubler Tensile Stress		Ultimate Doubler Shear Stress		Ultimate Doubler Bearing Stress	
		f_{ibu} (psi)	MS_{su}	f_{tu} (psi)	MS_{tu}	f_{tu} (psi)	MS_{tu}	f_{su} (psi)	MS_{su}	f_{bru}	MS_{bru}
	1	64.5	14.50	21,250	1.12						
A						59,794	1.96	21,177	4.43	203,300	.74
	2	84.0	10.90	53,736	3.09						
B						56,466	2.13	18,792	5.12	156,600	1.26
	3	48.0	19.83	26,613	.69						
C						31,109	4.69	10,110	10.37	70,100	4.05
	4	36.0	26.78	31,841	.41						
D						29,188	5.06	8,241	12.95	46,700	6.58
	5	73.5	12.60	37,865	.19						
E						8,738	19.26	8,738	12.16	11,650	29.38
E						8,738	19.26	8,738	12.16	11,650	29.38
	5	73.5	12.60	37,865	.19						
D						29,188	5.06	8,241	12,95	46,700	6.58
	4	36.0	26.78	31,841	.41						
C						31,109	4.69	10,110	10.37	70,100	4.05
	3	48 0	19.83	26,613	.69						
B						56,466	2.13	18,792	5.12	156,600	1.26
	2	84.0	10.90	53,736	3.09						
A						59,794	1.96	21,177	4.43	203,300	.74
	1	64.5	14.50	21,250	1.12						

The double shear area of the bolt is

$$A_s = \frac{2\pi}{4} d^2$$

$$A_s = \frac{2\pi(.375)^2}{4}$$

$$A_s = .2209 \text{ in.}^2$$

The ultimate shear stress is then

$$f_{su} = \frac{P_u}{A_s}$$

$$f_{su} = \frac{15,000}{.2209}$$

$$f_{su} = 67,904 \text{ psi}$$

For an ultimate shear strength, F_{su} = 95,000 psi, the ultimate margin of safety is

$$MS_{su} = \frac{95,000}{67,904} - 1 = \underline{.40}$$

The critical bolt bearing area is

$$A_{br} = 2t_d$$

$$A_{br} = 2(.30)(.375) = .225$$

and the ultimate bearing stress is

$$f_{bru} = \frac{P_u}{A_{br}}$$

$$f_{bru} = \frac{15,000}{.225}$$

$$f_{bru} = 66,667 \text{ psi}$$

Using the allowable ultimate bearing stress for the bolt material, F_{bru} = 219,000 psi, the margin of safety for the ultimate bearing is

$$MS_{bru} = \frac{219,000}{66,667} - 1 = \underline{2.28}$$

Elastic Pitch Beam Root End

The root end of the Elastic Pitch Beam, as it emerges from the hub, is critical for the 120-knot high-speed level-flight condition. Steady and vibratory components of inplane bending moment, steady and vibratory components of out-of-plane bending moment, and steady centrifugal force associated with the normal rotor speed of 2627 rpm are reacted at this location. The value of normal centrifugal force acting at the root end is obtained from Figure 12 by adding the total centrifugal force of the airfoil section to the centrifugal force of the Elastic Pitch Beam at this location. Values for the steady and vibratory inplane bending moments acting at the root end are obtained by aeroelastic analysis, the results of which are shown in Figure 15.

Steady and vibratory components of the out-of-plane bending moments acting at the root end of the Elastic Pitch Beam were obtained by a combination of two methods that incorporate the use of theoretical formulae and experimental test results. The steady coning and vibratory flapping angles for the 120-knot high-speed level-flight condition were first conservatively approximated by an aeroelastic analysis that assumed the blades to be freely articulated about the flapping axis at the elastomeric pivot. Out-of-plane bending moments acting on the Elastic Pitch Beam were then determined by assuming that the slope and deflection of the outboard attachment area of the Elastic Pitch Beam are equal to those of the airfoil section at the same location. Corrections to these results were made by using the experimental measured hub moment versus flapping angle relationship obtained for the UH-1 EPBTR, Reference 1. The procedure used is shown in the following:

The free-body sketch of the loads applied and their reactions is shown in Figure 16.

From tension-beam theory the slope at the outboard end of the Elastic Pitch Beam can be expressed as

$$\beta = \frac{V}{CF}\left[\frac{\text{Cosh}\lambda L - 1}{\text{Cosh}\lambda L}\right] - \frac{M\lambda}{CF}\,\text{Tanh}\lambda L \qquad (1)$$

where $\lambda = (CF/EI_{XX})^{\frac{1}{2}}$

and the deflection at the outboard end of the Elastic Pitch Beam can be expressed as

$$\delta = \frac{VL}{CF}\left[\frac{1-\text{Tanh}\lambda L}{\lambda L}\right] - \frac{M}{CF}\left[\frac{\text{Cosh}\lambda L - 1}{\text{Cosh}\lambda L}\right] \qquad (2)$$

From Figure 16, it is noted that the deflection δ can also be expressed as

$$\delta = L \text{ Tan } \beta \qquad (3)$$

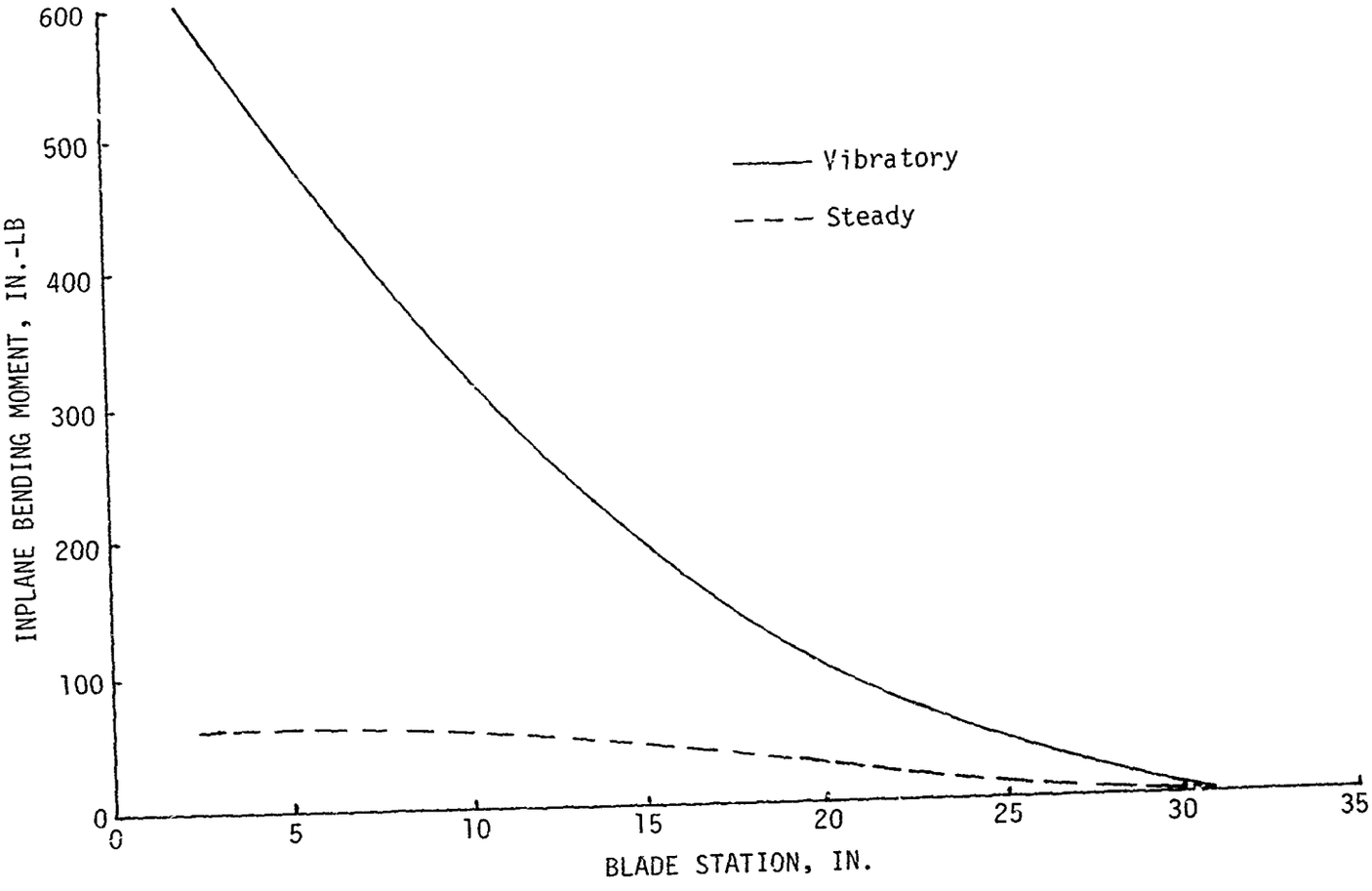

Figure 15. Steady and Vibratory Inplane Bending Moment Distribution for OH-58A Elastic Pitch Beam Tail Rotor.

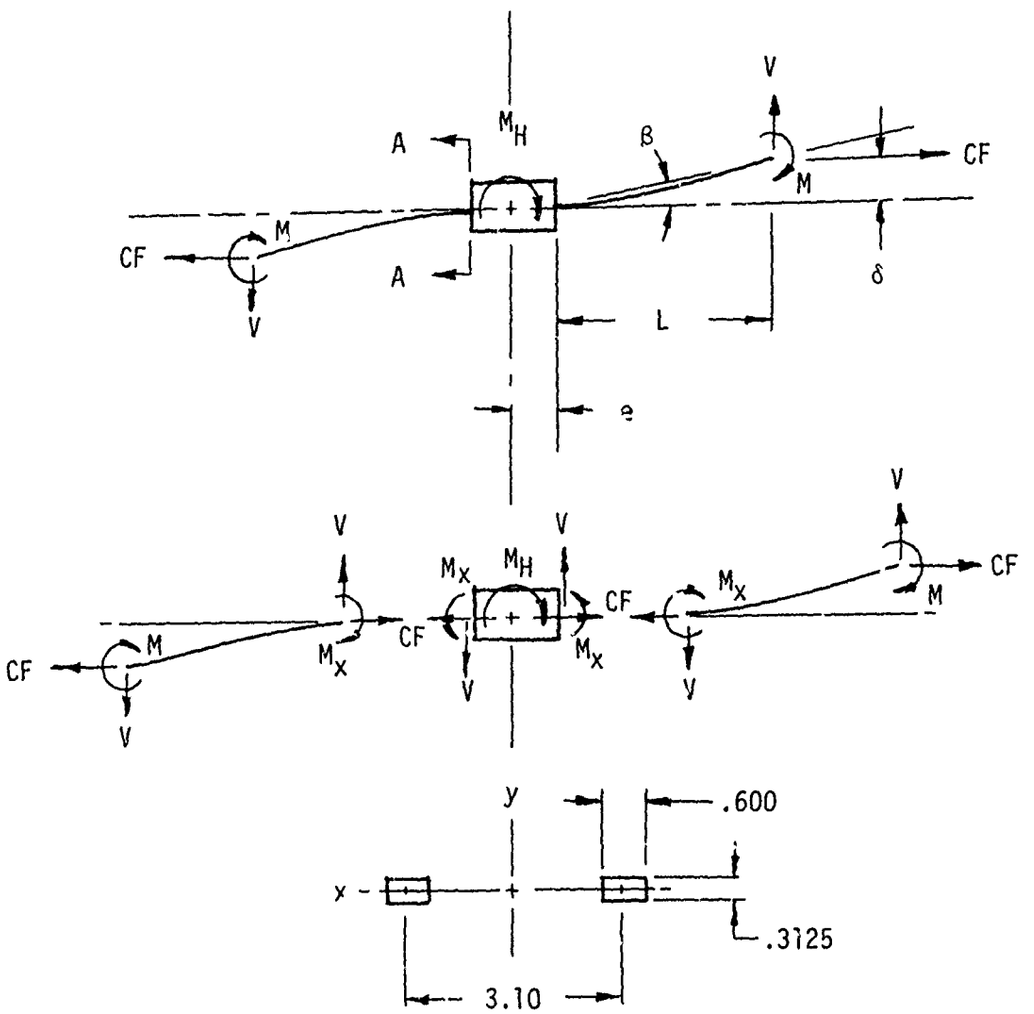

Section A-A

Figure 16. Out-of-Plane Loads and Reactions on Elastic Pitch Beam.

Substituting equation (3) into equation (2),

$$L \text{ Tan } \beta = \frac{VL}{CF}\left[\frac{1-\text{Tanh}\lambda L}{\lambda L}\right] - \frac{M}{CF}\left[\frac{\text{Cosh}\lambda L - 1}{\text{Cosh}\lambda L}\right] \quad (4)$$

Equations (1) and (4) were solved simultaneously for values of M and V in terms of the angle β by the use of a computer program called TENBM.

From Figure 16, the root end cut-of-plane bending moment acting on tne Elastic Pitch Beam is

$$M_X = VL - CF\delta - M \quad (5)$$

or using equation (3),

$$M_X = VL - CF \cdot L \text{ Tan } \beta - M \quad (6)$$

An expression relating the root end moment and shears of the Elastic Pitch Beam, M_X and V, to the hub moment, M_H, may also be derived from Figure 16.

$$M_H = 2M_X + 2Ve \quad (7)$$

Figure 17 shows the hub moment versus flapping angle relationship obtained experimentally for the UH-1 EPBTR.

Substituting the following UH-1 EPBTR parameters in Equations (1), (4), and (7) for a unit angle β,

$$CF = 12{,}500 \text{ lb}$$

$$L = 10 \text{ in.}$$

$$EI_{XX} = 95{,}800 \text{ lb-in.}^2$$

$$\beta = 1.0 \text{ deg}$$

$$e = 3.0 \text{ in.}$$

it is found that

$$M_H = 2728 \text{ in.-lb/deg}$$

which is the same as saying that the theoretical value of

$$K_{\beta T} = \frac{M_H}{\beta} = 2728 \text{ in.-lb/deg}$$

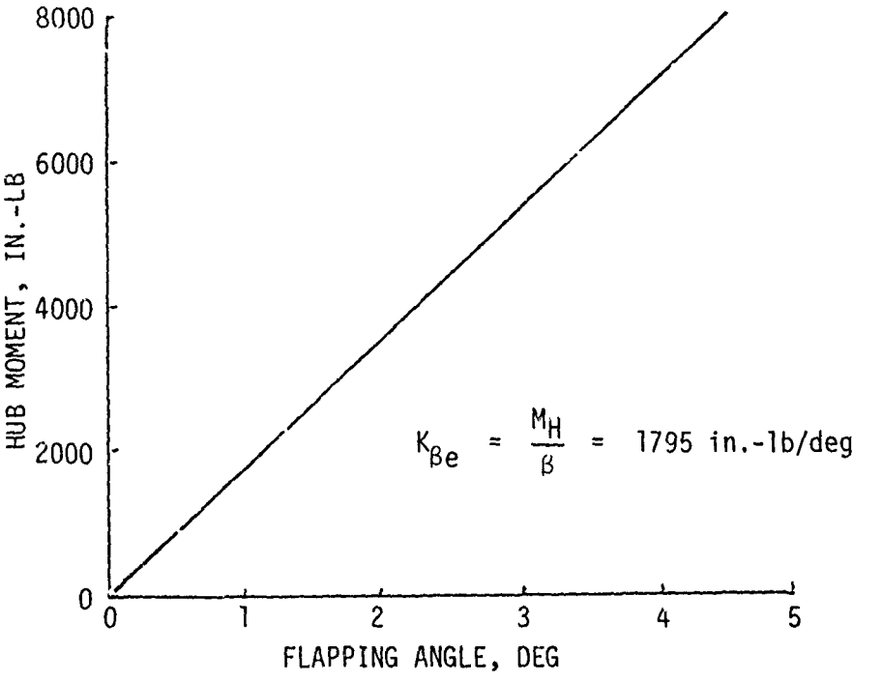

Figure 17. Flapping Spring Rate for UH-1 Elastic Pitch Beam Tail Rotor (Reference 1).

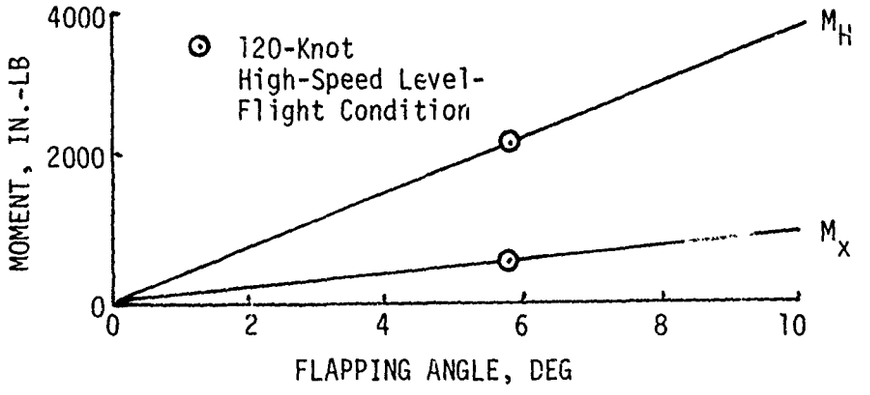

Figure 18. Root-End and Hub Moments for LOH Elastic Pitch Beam.

Since the experimental value of $K_{\beta e}$ was determined to be equal to 1795 in.-lb/deg from Figure 17, an empirical correction must be applied to the theoretical results of these equations. The value of this correction is

$$Z = \frac{K_{\beta e}}{K_{\beta T}} = \frac{1795}{2728}$$

$$Z = .6580$$

Substituting the following LOH Elastic Pitch Beam parameters into equations (1), (4), (6) and (7) and applying the corrector Z,

$$CF = 5050 \text{ lb}$$

$$L = 9.813 \text{ in.}$$

$$EI_{XX} = 21{,}361 \text{ lb-in.}^2$$

$$\beta = \pm 5.78 \text{ deg}$$

$$e = 1.187 \text{ in.}$$

$$Z = .6580$$

Values of M_X and M_H obtained for the 120-knot high-speed level-flight condition ($\beta = \pm 5.78$ degrees) are

$$M_X = \pm 570 \text{ in.-lb}$$

$$M_H = \pm 2108 \text{ in.-lb}$$

Figure 18 presents the values of M_X and M_H for other flapping angles.

The primary loads acting on the root end of the Elastic Pitch Beam during the 120-knot high-speed level-flight condition are then

$$CF = 5050 \text{ lb} \qquad \text{(Figure 12)}$$

$$M_X = \pm 570 \text{ in.-lb} \qquad \text{(Figure 13)}$$

$$M_y = 60 \pm 580 \text{ in.-lb} \qquad \text{(Figure 15)}$$

The stresses resulting from these loads are determined from the following expression for combined stress:

$$f_b = \frac{CF \cdot E}{\Sigma EA} + \frac{M_X C_y E}{\Sigma EI_{XX}} + \frac{M_y C_X E}{\Sigma EI_{yy}}$$

Using values of ΣEA, ΣEI_{xx}, ΣEI_{yy}, C_y, and C_x, from Figures 7, 8, 9, and 16, the combined stress is then

$$f_b = \frac{5050\ (7.0 \times 10^6)}{2.625 \times 10^6} \pm \frac{570(.1562)(7.0 \times 10^6)}{.0214 \times 10^6}$$

$$+ \frac{(60 \pm 580)(1.70)(7.0 \times 10^6)}{5.166 \times 10^6}$$

$$f_b = 13{,}605 \pm 30{,}459 \text{ psi}$$

Figure 19 presents the fatigue test results obtained for the root end of the 3M-1002-1014 "S" glass UH-1 Elastic Pitch Beam, References 1 and 2. For a steady stress of 25,000 psi, the allowable vibratory stress, F_a, for this material is 38,000 psi. Applying the Goodman diagram correction to account for the lower steady stress in the LOH Elastic Pitch Beam, the allowable vibratory stress for a steady stress of 13,605 psi is F_a = 40,221 psi. The margin of safety for the vibratory stress is then

$$MS_f = \frac{F_a}{f_v} - 1$$

$$MS_f = \frac{40{,}221}{30{,}459} - 1$$

$$MS_f = \underline{\underline{.32}}$$

Airfoil Section

The airfoil section of the LOH Elastic Pitch Beam tail rotor is critical for the 120-knot high-speed level-flight condition. Centrifugal force due to normal rotor speed, steady and vibratory inplane bending moments, and steady and vibratory out-of-plane bending moments are the principal loads acting on the airfoil section for this condition. The spanwise distribution of centrifugal force is shown in Figure 12. Steady and vibratory inplane bending moments are shown in Figure 15, and steady and vibratory out-of-plane bending moments are shown in Figure 20.

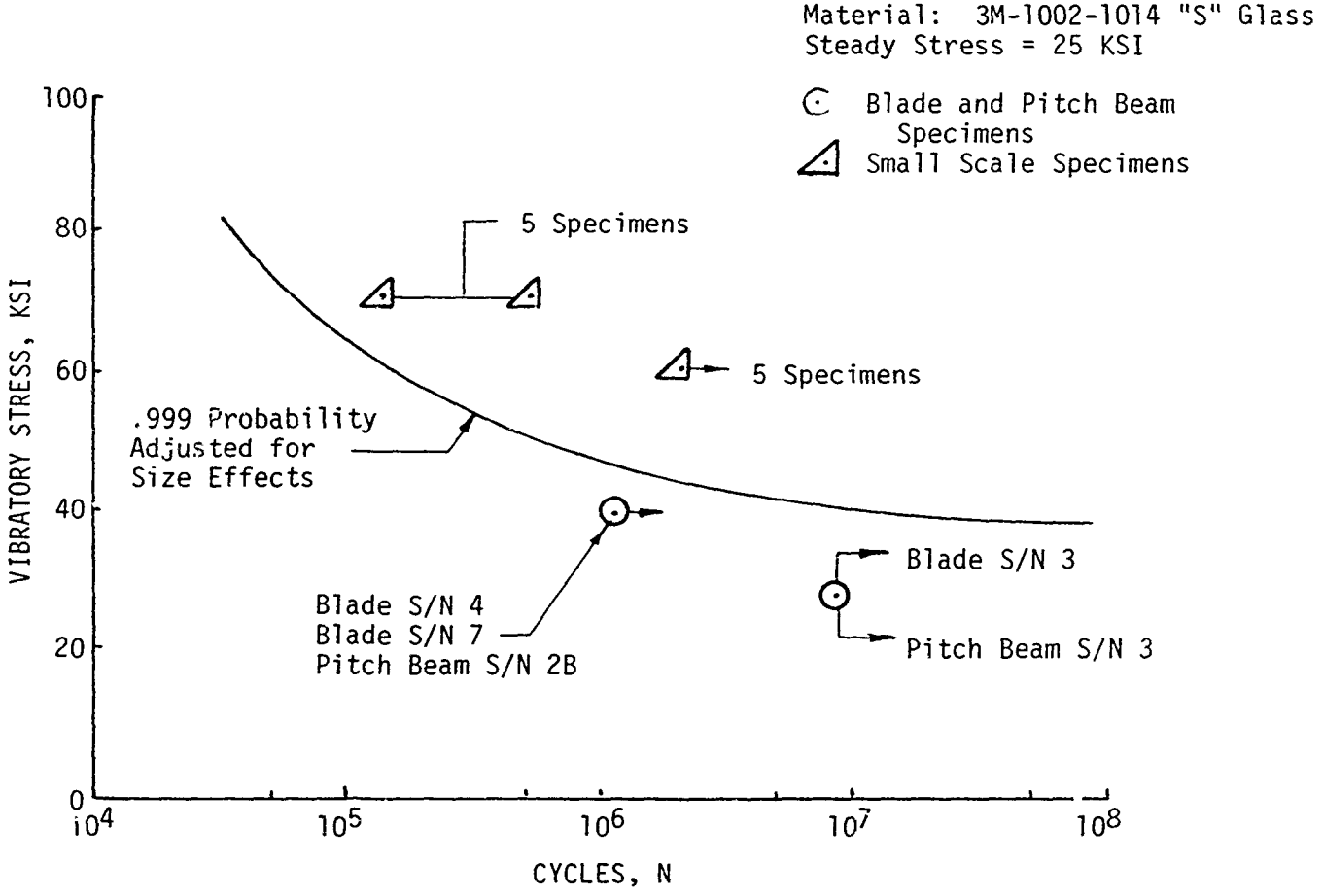

Figure 19. S-N Curve for Root End of UH-1 Elastic Pitch Beam (References 1 and 2).

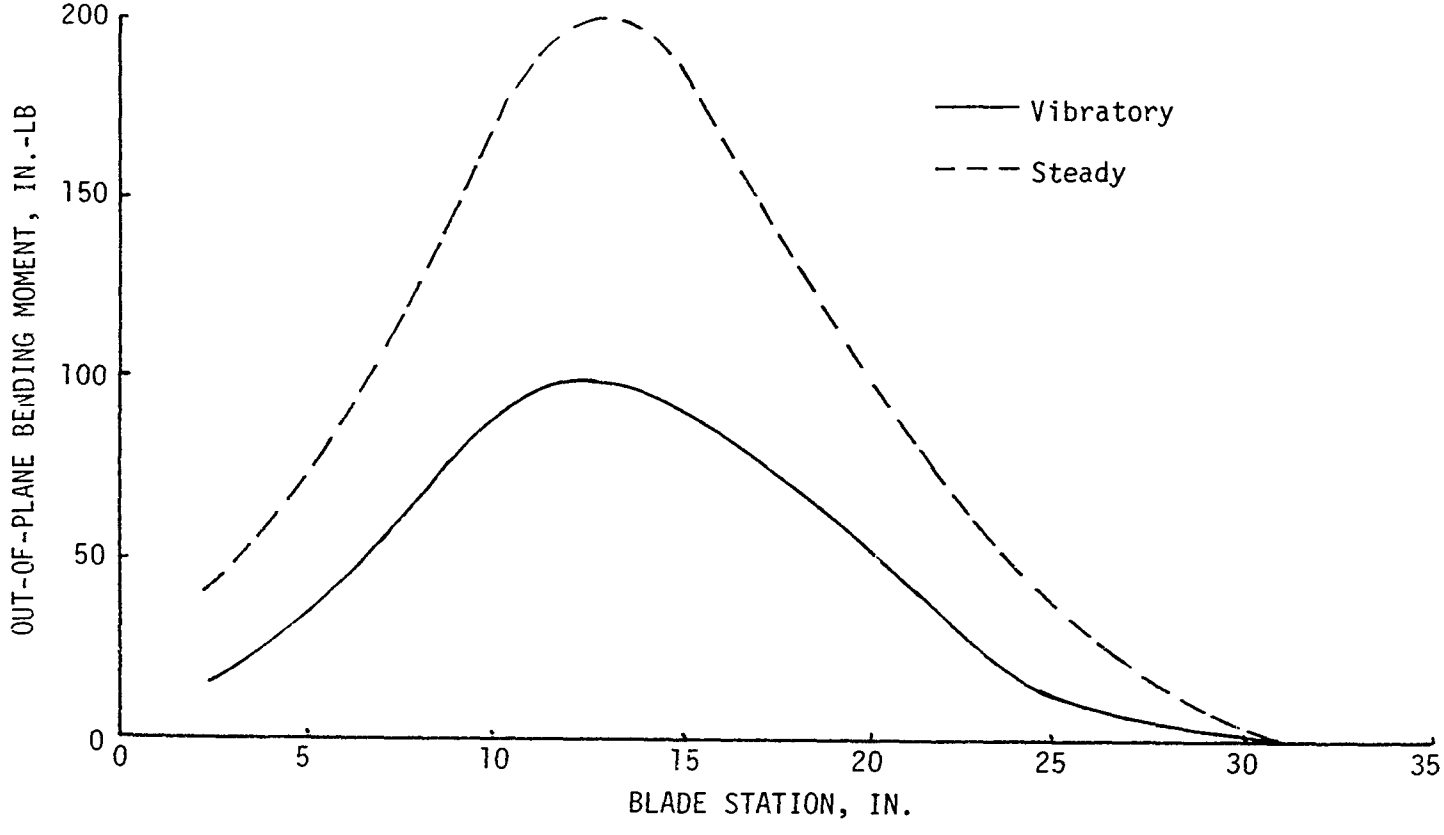

Figure 20. Steady and Vibratory Out-of-Plane Bending Moment Distribution for OH-58A Elastic Pitch Beam Tail Rotor.

Station 14.5, the location of high flatwise bending moments and relatively low section properties, is considered to be the critical airfoil section station.

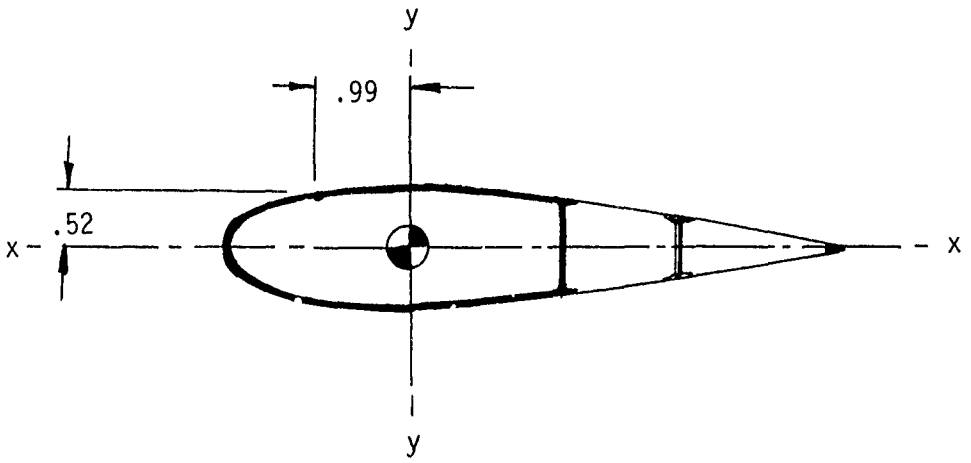

Figure 21. Airfoil Section at Station 14.5.

The loads acting at Station 14.5 are

CF	=	2700 lb	(Figure 12)
M_y	=	50 $\pm$ 200 in.-lb	(Figure 15)
M_x	=	200 $\pm$ 100 in.-lb	(Figure 20)

and the pertinent section properties at Station 14.5 are

ΣEA	=	2.63×10^6 lb	(Figure 7)
ΣEI_{yy}	=	3.12×10^6 lb-in.^{2}	(Figure 8)
ΣEI_{xx}	=	$.13 \times 10^6$ lb-in.^{2}	(Figure 9)
C_y	=	.52 in.	(Figure 21)
C_x	=	.99 in.	(Figure 21)

Material properties for the BP 919/7581 glass composite are, from References 5 and 6,

$$F_{tu} = 45{,}000 \text{ psi}$$

$$E = 3{,}200{,}000 \text{ psi}$$

$$F_e = 10{,}000 \text{ psi}$$

The combined stress at this location is determined by

$$f_b = \frac{CF(E)}{\Sigma EA} + \frac{M_y C_x E}{\Sigma EI_{yy}} + \frac{M_x C_y E}{\Sigma EI_{xx}} = f_s \pm f_v$$

where f_s and f_v are the steady and vibratory component of the combined stress

$$f_b = \frac{2700(3.2 \times 10^6)}{2.63 \times 10^6} + \frac{(50 \pm 200)(.99)(3.2 \times 10^6)}{3.12 \times 10^6} + \frac{(200 \pm 100)(.52)(3.2 \times 10^6)}{.930 \times 10^6}$$

$$f_b = 3285 + 51 \pm 203 + 358 \pm 179$$

$$f_b = f_s \pm f_v = 3694 \pm 382 \text{ psi}$$

The allowable vibratory stress, considering the Goodman diagram correction for steady stress, is

$$F_a = F_e\left(1 - \frac{f_s}{F_{tu}}\right)$$

$$F_a = 10{,}000\left(1 - \frac{3694}{45{,}000}\right)$$

$$F_a = 9179 \text{ psi}$$

The margin of safety for fatigue is then

$$MS_f = \frac{F_a}{f_v} - 1$$

$$MS_f = \frac{9179}{382} - 1 = \underline{\underline{23.03}}$$

$$\underline{\underline{\text{Ample}}}$$

Hub Trunnion

A conservative analysis of the bending stresses imposed on the hub trunnion can be made by assuming that the inplane and out-of-plane moments acting at the attachment point to the Elastic Pitch Beam, Station 11.0, are reacted by inplane and out-of-plane shear loads passing through the elastomeric pivot into the hub trunnion at Station 1.80 as shown in Figure 22.

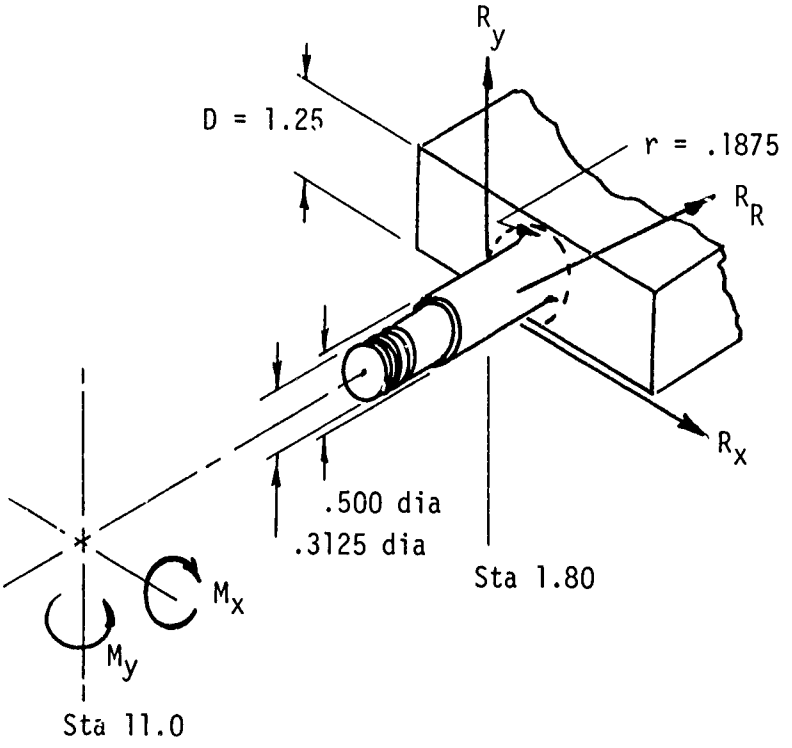

Figure 22. Hub Trunnion Loads.

The moment of inertia of the hub trunnion at Station 1.80 is

$$I = \frac{\pi d^4}{64} = \frac{\pi(.500)^4}{64}$$

$$I = .0031 \text{ in.}^4$$

Bending moments at Station 11.0 for the 120-knot high-speed level-flight condition are

$M_x = 200 \pm 100$ in.-lb (Figure 20)

$M_y = 53 \pm 295$ in.-lb (Figure 15)

The reactions at the hub trunnion, Station 1.80, are

$$R_x = \frac{My}{L} = \frac{53 \pm 295}{9.20} = 6 \pm 32 \text{ lb}$$

$$R_y = \frac{Mx}{L} = \frac{200 \pm 100}{9.20} = 22 \pm 11 \text{ lb}$$

The resultant reaction at the hub trunnion is

$$R_R = (R_x^2 + R_y^2)^{\frac{1}{2}}$$

$$R_R = [(6 \pm 32)^2 + (22 + 11)^2]^{\frac{1}{2}}$$

$$R_R = 22.8 \pm 33.8 \text{ lb}$$

The bending moment at the root of the trunnion, Station 1.20, is

$$M = (1.8 - 1.2)(R_R)$$

$$M = .6(22.8 \pm 33.8)$$

$$M = 13.7 \pm 20.3 \text{ in.-lb}$$

The stress concentration factor, K_t, for the hub trunnion root is found in Reference 7 for the following relationships:

$$\frac{r}{d} = \frac{.1875}{.50} = .375$$

$$\frac{D}{d} = \frac{1.25}{.5} = 2.5$$

$$K_t = 1.20$$

The combined stress, and the steady and vibratory components of the combined stress, are found to be

$$f_b = f_s + f_v - (M_s + K_t M_v) \frac{c}{I}$$

$$f_b = f_s + f_v = [13.7 \pm 1.2(20.3)] \frac{.25}{.0031}$$

$$f_b = f_s + f_v = 1105 \pm 1964 \text{ in.-lb}$$

The allowable vibratory stress, F_a, is obtained by applying the Goodman diagram correction for steady stress:

$$F_a = F_e\left(1 - \frac{f_s}{F_{tu}}\right)$$

Using F_{tu} = 155,000 psi for 15-5PH stainless steel, Condition H 1025 and F_e = 18,000 psi,

$$F_a = 18{,}000\left(1 - \frac{1105}{155{,}000}\right)$$

$$F_a = 17{,}872 \text{ psi}$$

The margin of safety in fatigue is then

$$MS_f = \frac{F_a}{f_v} - 1$$

$$MS_f = \frac{17{,}872}{1964} - 1$$

$$MS_f = \underline{\underline{8.10}}$$

Fail-Safe Provisions

As shown in Figure 2, provisions have been incorporated in the design of the LOH Elastic Pitch Beam tail rotor to provide an alternate load path to carry the airfoil section centrifugal force (normally carried by the EPB) into the tail rotor hub and shaft. This load path would be used only in the event that an airfoil section moved outward relative to the hub due to a partial failure of the EPB or a bond failure between the hub, hub elastomer, or EPB. If one of these conditions should materialize, the outward motion of the airfoil section would be limited by the bearing retainer coming into contact with the fail-safe - flapping stop mounted on the hub trunnion. Under these circumstances, the centrifugal force of the airfoil section would be carried by the airfoil section leading-edge spar, the bond between the airfoil section leading-edge spar and the inboard fitting, through the two bolts attaching the bearing housing and retainer to the inboard fitting, and through the fail-safe - flapping stop into the hub trunnion. The following stress analysis demonstrates the adequacy of the structure forming this alternate load path for carrying the 4250-pound normal centrifugal force of the airfoil section obtained from Figure 12.

1. Tensile Strength of Glass Composite Spar

The ultimate tensile strength of the inboard portion of the airfoil section at Station 3.75 is determined by assuming that the axial load carried by the six plies of BP 919/7581 "E" glass and the two plies of 3M-1002-1014 "S" glass is proportional to their axial stiffnesses (EA).

Material	t	E	A	EA
BP 919/7581	.060	3.2×10^6	.598	1.914×10^6
3M 1002-1014	.020	7.0×10^6	.199	1.393×10^6
	.080	---	.797	3.307×10^6

The tensile stress in each material is determined from

$$f_t = \frac{CF\ E}{\Sigma EA} = \frac{4250(3.2 \times 10^6)}{3.307 \times 10^6}$$

$$f_t = 4112 \text{ psi}$$

F_{tu} = 45,000 psi (Reference 5)

$$MS_t = \frac{F_{tu}}{f_t} - 1 = \frac{45{,}000}{4112} - 1$$

MS_t = 9.94 Ample

For 3M-1002-1014 "S" glass,

$$f_t = \frac{CF\ E}{\Sigma EA} = \frac{4250(7.0 \times 10^6)}{3.307 \times 10^6}$$

$$f_t = 8996 \text{ psi}$$

F_{tu} = 220,000 psi

$$MS_t = \frac{F_{tu}}{f_t} - 1 = \frac{220{,}000}{8996} - 1$$

MS_t = 23.46 Ample

2. Bond of the Airfoil Section to the Inboard Fitting

Bond area:

$$A_s = 21.87 \text{ in.}^2$$

Bond stress:

$$f_s = \frac{CF}{A_s} = \frac{4250}{21.87}$$

$$f_s = 194 \text{ psi}$$

A conservative estimate of the bond strength of Plastilock 717 adhesive is F_{su} = 1000 psi. The margin of safety is then

$$MS_s = \frac{F_{su}}{f_s} - 1 = \frac{1000}{194} - 1$$

$$MS_s = \underline{4.15}$$

3. Attachment of Inboard Fitting to Bearing Retainer and Bearing Housing

Two NAS 464-4 bolts, or equivalent, will be used to attach the bearing retainer and housing to the inboard fitting, F_{tu} = 160,000 psi.

Area of bolt at thread root:

$$A_t = .0326 \text{ in.}^2$$

The tensile stress in the bolts is

$$f_t = \frac{CF}{2A_t} = \frac{4250}{2(.0326)}$$

$$f_t = 65{,}184 \text{ psi}$$

and the margin of safety in tension is

$$MS_t = \frac{F_{tu}}{f_t} - 1 = \frac{160{,}000}{65{,}184} - 1$$

$$MS_t = \underline{1.45}$$

4. Hub Trunnion

The structural adequacy of the hub trunnion for resisting the normal centrifugal force of 4250 pounds applied during the fail-safe condition can be demonstrated by superimposing the steady axial stress due to this load on the stresses previously determined at Station 1.2 for the 120-knot high-speed level-flight condition, and by checking the tensile strength of the 5/16-24UNF-3A thread located at the outer end of the hub trunnion.

Hub trunnion bending stresses at Station 1.2 previously determined are

$$f_b = f_s + f_v$$

$$f_b = 1105 \pm 1964 \text{ in.-lb}$$

The additional steady stress to be added due to the 4250-pound centrifugal force load is

$$f_s = \frac{CF}{A_t} \qquad \text{where}$$

$$A_t = \frac{\pi d^2}{4} = \frac{\pi(.500)^2}{4}$$

$$A_t = .1964 \text{ in.}^2$$

Then the steady stress component, f_s , is

$$f_s = \frac{4250}{.1964}$$

$$f_s = 21{,}639 \text{ psi}$$

The total combined stress acting at Station 1.2 is then

$$f_b = f_s + f_v = 21{,}639 + 1105 \pm 1964$$

$$f_b = f_s + f_v = 22{,}744 \pm 1964 \text{ psi}$$

The allowable vibratory stress, F_a, is (using F_e = 18,000 psi)

$$F_a = F_e \left(1 - \frac{f_s}{F_{tu}}\right)$$

$$F_a = 18{,}000 \left(1 - \frac{22{,}744}{155{,}000}\right)$$

$$F_a = 15{,}359 \text{ psi}$$

The margin of safety in fatigue is

$$MS_f = \frac{F_a}{f_v} - 1 = \frac{15{,}359}{1964} - 1$$

$$MS_f = \underline{\underline{6.82}}$$

For the 5/16-24UNF-3A thread at the outer end of the hub trunnion, the root area of the thread is

$$A_r = .0524 \text{ in.}^2$$

and the tensile stress is

$$f_t = \frac{CF}{A} = \frac{4250}{.0524}$$

$$f_t = 81{,}107 \text{ psi}$$

For F_{tu} = 115,000 psi (15-5PH stainless steel),

$$MS_t = \frac{F_{tu}}{f_t} - 1 = \frac{155{,}000}{81{,}107} - 1$$

$$MS_t = \underline{\underline{.90}}$$

Tail Rotor Shaft

The teeter freedom of the current OH-58A tail rotor has been eliminated in the design of the LOH Elastic Pitch Beam tail rotor to improve the reliability and maintainability of this system through design simplification and through the elimination of troublesome teeter bearings. Vibratory hub moments developed in the proposed semirigid rotor system resulting from blade flapping in forward flight must now be resisted by the current OH-58A tail rotor shaft. As this shaft was not originally designed to resist vibratory hub moments, some degradation in its fatigue life is anticipated. The degree to which the tail rotor shaft's capabilities will be affected by the vibratory hub moment cannot be predicted with a high degree of confidence due to the lack of available data on which such a judgement should be based. A qualitative estimate, however, can be made if it is assumed that the endurance limit of the tail rotor shaft, F_e, is 25,000 psi, and that the section properties at its critical cross section, just inboard of the tail rotor hub attachment spline, are approximately

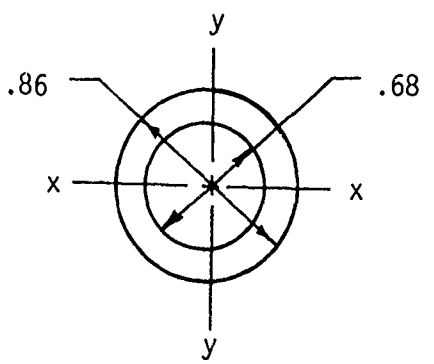

$$A = \frac{\pi}{4}(d_o^2 - d_i^2)$$

$$A = \frac{\pi}{4}\left[(.86)^2 - (.68)^2\right]$$

$$A = .2177 \text{ in.}^2$$

$$I_{xx} = I_{yy} = \frac{\pi}{64}(d_o^4 - d_i^4) = \frac{\pi}{64}\left[(.86)^4 - (.68)^4\right]$$

$$I_{xx} = I_{yy} = .0164 \text{ in.}^4$$

Further assuming that the effects of the steady stresses due to torque and thrust at this location are relatively low, the allowable vibratory hub moment permitted without exceeding the endurance limit can be approximated by

$$M_{H_{max}} = \frac{F_e I_{xx}}{C_y} = \frac{25{,}000(.0164)}{.43}$$

$$M_{H_{max}} = 953 \text{ in.-lb}$$

Figure 23 shows the allowable hub moment for infinite life plotted with the hub moment - flapping angle relationship previously determined from Figure 18. Also shown is the estimated hub moment for the 120-knot high-speed level-flight condition. Figure 23 indicates that the current OH-58A tail rotor shaft will not incur any fatigue damage for flight conditions having vibratory flapping angles less than approximately ± 2.75 degrees. Fatigue damage will accumulate, however, during those flight conditions having flapping angles higher than the ± 2.75 degrees allowable. As the flapping angle associated with the 120-knot high-speed level-flight condition is higher than the allowable flapping angle, it is anticipated that some restrictions to the present OH-58A flight envelope may be required when flight testing the proposed LOH Elastic Pitch Beam tail rotor defined herein. The degree of these restrictions can be ascertained only after the fatigue strength of the tail rotor shaft subjected to vibratory hub moments has been determined, flight loads associated with the anticipated flight envelope have been obtained, and the flight loads spectrum has been defined.

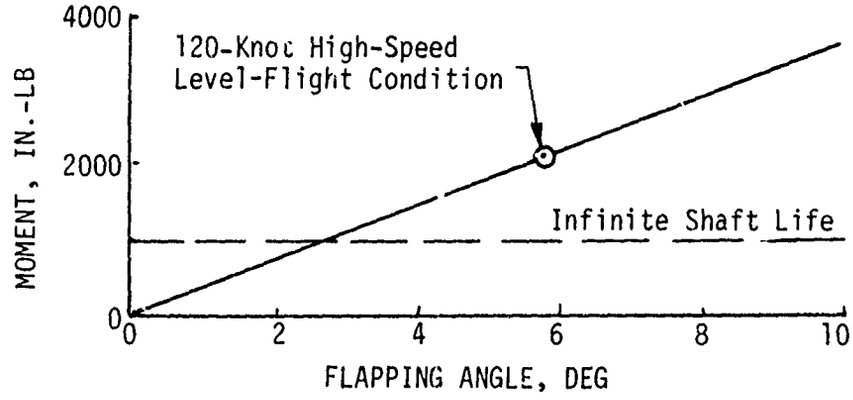

Figure 23. Hub Moment Applied to Current OH-58A Tail Rotor Shaft Versus Flapping Angle.

ELASTIC PITCH BEAM TEST SPECIMEN

The Elastic Pitch Beam shown in Figure 2 and detailed in Figure 24 was fabricated and static tested to an axial load of 18,500 pounds without failure to demonstrate the adequacy of the Elastic Pitch Beam - airfoil section attachment. The ultimate centrifugal force load acting at this interface is 8550 pounds but the attachment was conservatively designed for an ultimate load of 15,000 pounds, to allow for possible increases in load due to design changes. A description of the fabrication and test procedures and results are presented in the following.

SPECIMEN FABRICATION

Unidirectional 3M-1002-1014 "S" glass epoxy "B" stage tapes, 17-7PH stainless steel doublers, 6061-T6 aluminum cheek plates, and Plastilock 717 .030 lb/sq ft unsupported film adhesive were the basic materials used to fabricate the Elastic Pitch Beam test specimen shown in Figure 24. The unidirectional "S" glass tapes, .600 inch wide and approximately .010 inch thick, were initially shaped to conform to the planform configuration of the two EPB truss members so that the glass filaments in each tape were approximately parallel to the inner and outer edges of the truss members. Stainless steel doublers and aluminum cheek plates were machined, vapor blasted, etched and primed with Plastilock 718-2 primer.

The full-length mold used to form and cure the EPB assembly is "split" at its midplane to form upper and lower mold halves comprised of window-frame sections conforming to the outer planform surfaces of the EPB and wedge-shape sections conforming to the inner planform surfaces of the EPB. Initially, the upper mold-half was attached to a base plate and a nylon peel ply was laid in the bottom of the mold cavity. A .010-inch-thick stainless steel doubler, doubler F, was positioned at each end of the mold assembly, and a filler ply of unidirectional "S" glass ½ inch long was butted against the inboard edge of each of the .010-inch-thick doublers to serve as transition strips. Six preformed unidirectional "S" glass tapes, laminate number 4, were then laid in the mold cavity for each truss member. Six triangular shaped unidirectional "S" glass filler strips were laid between the two truss member at the outboard ends of the layup. Doublers E, .020 inch thick and having a ply of Plastilock 717 adhesive attached to both surfaces, were then positioned at each end in the mold cavity. A 5/8-inch and a ½-inch unidirectional "S" glass filler strip were butted to the inboard doubler edges at each end. This sequence of buildup was continued until the upper half of the Elastic Pitch Beam was completed. Contoured and formed .060-inch-thick aluminum caul plates were placed over the web truss members; then the assembly was placed in a vacuum bag and cured in an autoclave at a pressure of 40 psi and a temperature of $350^{o} \pm 10^{o}F$ for one hour at temperature. On completion of the cure, the mold base plate was removed, exposing the mid-chord plane of the upper EPB assembly. After the assembly was turned over, the nylon peel ply was stripped from the laminate and the

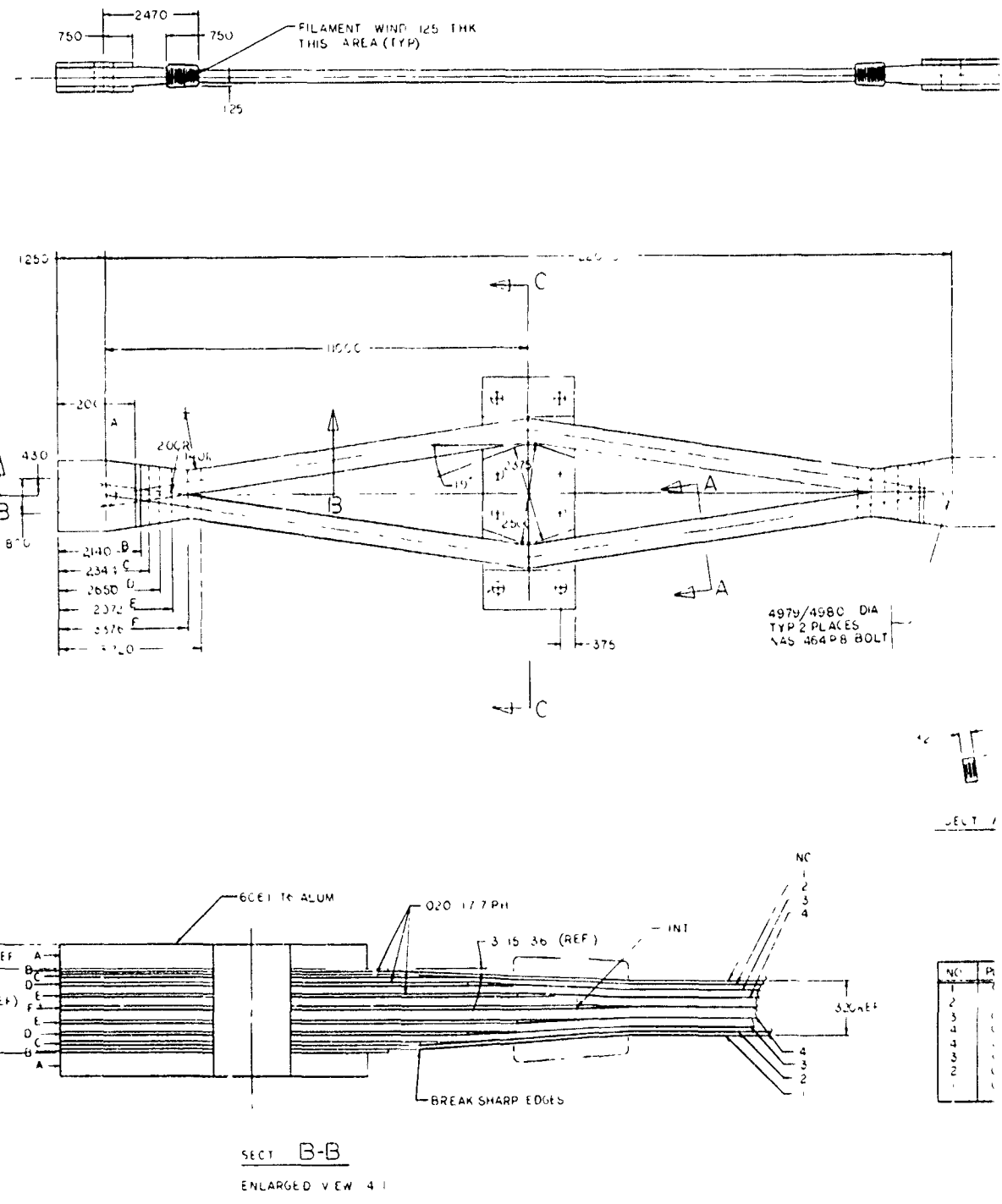

Figure 24. Test Specimen LOH Elastic Pitch Beam Tail Rotor.

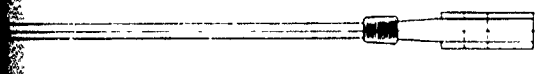

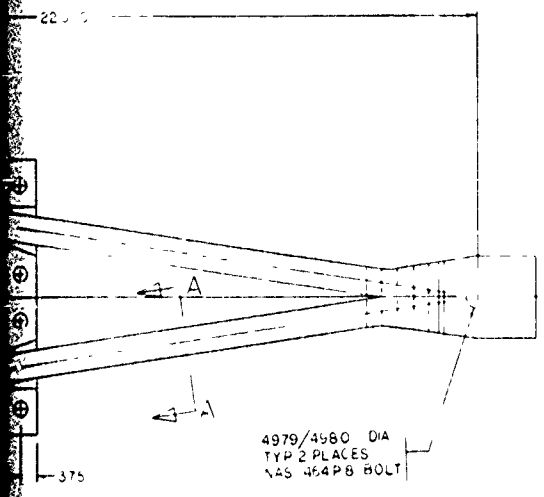

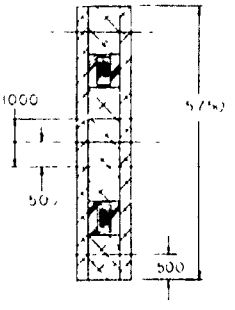

SECT C-C

SECT A-A

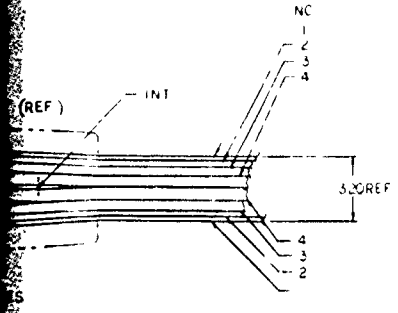

NC	PLY THK
1	025
2	.030
3	050
4	060
4	060
3	050
2	030
1	025

lower mold half was attached to the upper mold half. A ply of Plastilock 717 adhesive was positioned over the faying surface of the cured half of the Elastic Pitch Beam. Buildup of the remaining half of the Elastic Pitch Beam was identical to the upper half which on completion resulted in a symmetrical Elastic Pitch Beam structure. Caul plates were positioned on the uncured laminate, and the assembly was again placed in a vacuum bag and cured at a pressure of 40 psi and a temperature of $350^{o} + 10^{o}F$ for one hour at temperature. On completion of the cure, the Elastic Pitch Beam was removed, and filament winding was applied at each end as shown in Figure 24. The complete assembly was then placed in a $150^{o}F$ oven for 2 hours to cure the filament-wound areas. A picture of the completed Elastic Pitch Beam without the hub is shown in Figure 25.

The two-bladed elastomeric hub used for the static test specimen, shown in Figure 24, is similar to the one shown in Figure 2 except that modifications were incorporated to simplify its fabrication for use on the test specimen. As shown, the static test hub is composed of upper and lower cover plates, two end spacer blocks, a center form block configured to form the inner groove surfaces required for the Elastic Pitch Beam-hub attachment, and assembly bolts. After the Elastic Pitch Beam truss members were centered with respect to the hub and formed seals were positioned at the outboard edges of the hub, Furane Plastics 8615 Uralane adhesive (a urethane casting compound having a durometer of 50-60) was injected into the hub cavity. The complete Elastic Pitch Beam - hub assembly was then placed in an oven, and the Uralane was cured for 2 hours at $200^{o}F$.

SPECIMEN TESTING

Static tests were performed on the Elastic Pitch Beam test specimen to gain an insight into the performance characteristics of the design. Test procedures and test results obtained for torsional stiffness and tensile strength investigations are presented in the following.

Torsional Stiffness Versus Centrifugal Force

The torsional stiffness of the Elastic Pitch Beam test specimen was determined for several values of applied centrifugal force using the test setup shown in Figure 26. The outboard attachment ends of the test specimen were mounted in a Tinius Olsen test machine, and a crossbar was bolted to the center of the hub. Cables attached to the ends of the crossbar and running over pulleys to weight trays provided a means for applying a torsional moment to the test specimen. A deflection pointer attached to one end of the crossbar was used to indicate the angular displacement of the hub. Three torsional stiffness test runs were made: one without axial load, one having 6000 pounds of axial load, and one having 12,000 pounds of axial load. Results of these tests are shown in Figure 27.

As the torque-deflection relationships measured in these tests include the torsional stiffness of both ends of the Elastic Pitch Beam, the torsional stiffness for each blade would be half of the measured values as indicated

Figure 25. OH-58A Elastic Pitch Beam.

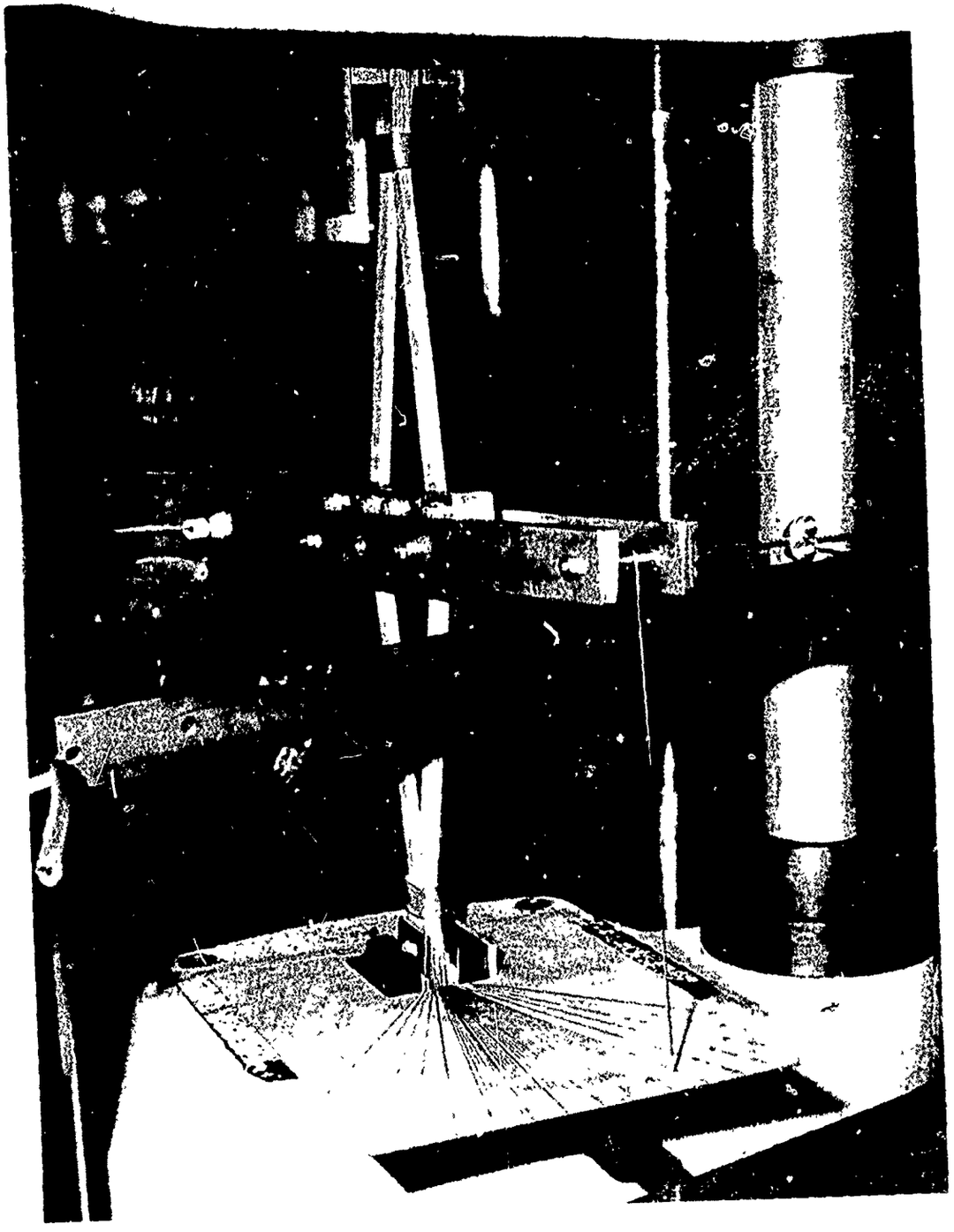

Figure 26. OH-58A Elastic Pitch Beam and Elastomeric Hub Mounted in Tinius Olsen Testing Machine for Torsional Stiffness and Tensile Tests.

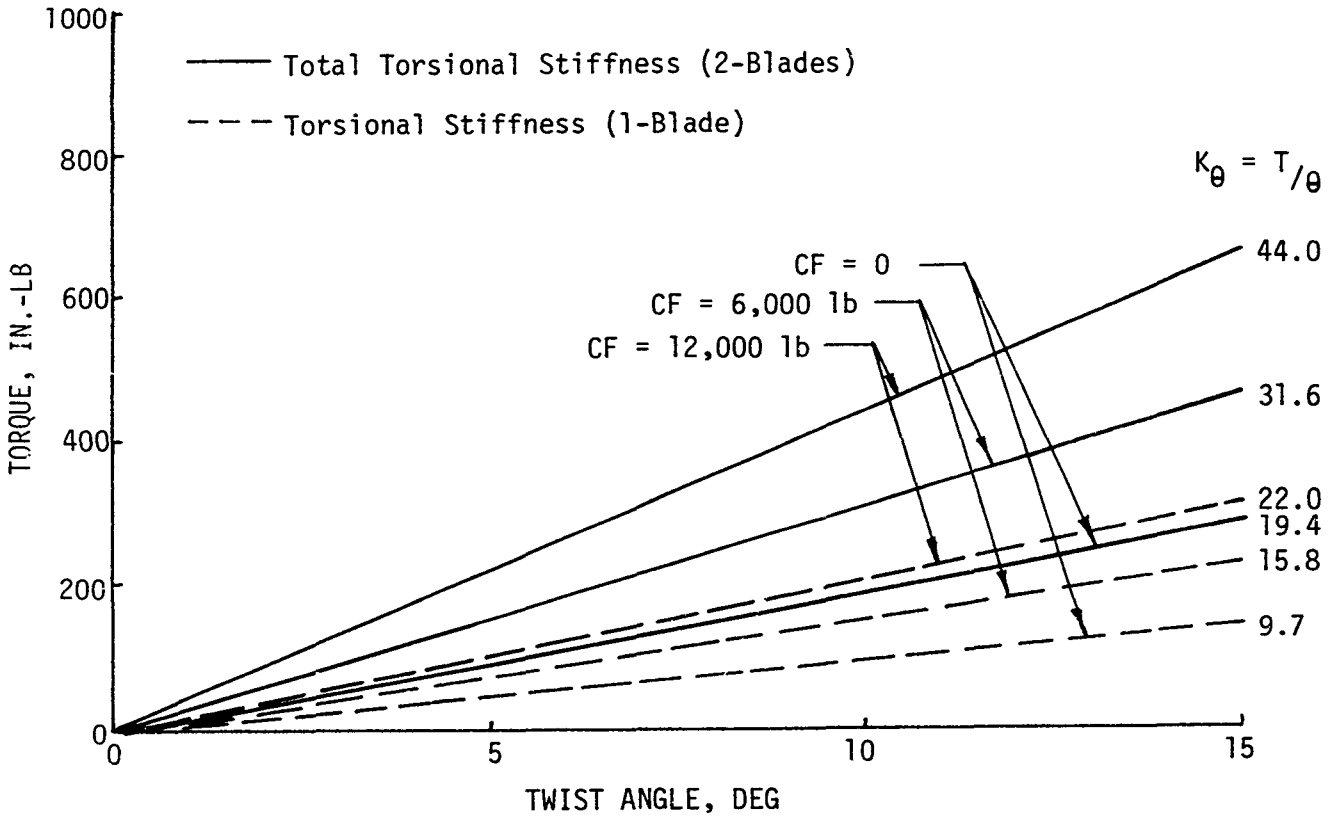

Figure 27. Torsional Stiffness Versus Centrifugal Force for Elastic Pitch Beam Test Specimen.

by the dashed lines in Figure 27. The centrifugal force acting at the outboard attachment end of the Elastic Pitch Beam for a normal rotor speed of 2627 rpm obtained from Figure 12 is 4200 pounds. The torsional stiffness of each end of the Elastic Pitch Beam that can be anticipated for this operating condition is then found to be 13.97 in.-lb/deg from Figure 27.

Tensile Strength

The tensile strength capabilities of the Elastic Pitch Beam test specimen were determined by mounting the specimen in the Tinius Olsen testing machine as shown in Figure 26. The hub was twisted through an angle of 12 degrees to simulate the maximum anticipated pitch angle of the Elastic Pitch Beam. (It should be noted that the airfoil sections attached to both ends of the Elastic Pitch Beam are aligned at 5 degrees to planform plane of the EPB so that during the required airfoil section pitch travel of -6 to +16.5 degrees, the required pitch range for the EPB is +11.25 degrees.) Axial load was applied up to 18,500 pounds without failure of the Elastic Pitch Beam. As this load is well above the 8550 ultimate design load, the adequacy of the Elastic Pitch Beam design for resisting the static loading has been demonstrated.

COST EFFECTIVENESS

The Elastic Pitch Beam tail rotor for the OH-58A has potential for a substantial improvement in the cost effectiveness of the tail rotor hub and blade. This is due to the high reliability and repairability, increased simplicity and damage resistance, and reduced maintenance requirements that can be realized through the EPBTR design. A measure of the cost effectiveness, or the cost saving potential, of the OH-58A EPBTR was obtained by using the life-cycle cost model of Reference 9. Previous experience with the use of this cost model has shown that the five main factors influencing helicopter rotor life-cycle costs are:

- Acquisition cost
- MTBR (mean time between failure)
- Field repairability on and off the aircraft
- Fatigue life
- Requirement for depot repair.

Table 5 presents the estimated acquisition costs for both the present OH-58A tail rotor and the EPBTR. The $778 for the present OH-58A tail rotor reflects the low cost that can be gained through large production runs of components that have been in use for several years. The cost estimate of $1431 for the EPBTR reflects the present cost of composite materials and present methods of composite component manufacturing. Over the past few years the cost of composite materials has been reduced and significant advances in automating composite manufacturing methods have been made. It is reasonable to assume that these two factors will continue to have a cumulative effect in reducing composite component prices in the future. For this analysis, however, the $1431 figure was used in determining the cost effectiveness of the EPBTR.

TABLE 5. COST SUMMARY FOR OH-58A TAIL ROTOR ASSEMBLIES FOR A PRODUCTION RATE OF 135 UNITS/MONTHS FOR 5 YEARS

Aircraft	Configuration	Hub or Hub & Pitch Spring	Two Tail Rotor Blades	Rotor Assembly
OH-58A	Production	250	528	778
	EPBTR	679	752	1431

An assessment of the MTBF (mean time between failure) may be obtained by examining the basic design features of the EPBTR and comparing them to those of the current OH-58A tail rotor. The EPBTR airfoil section, shown in Figure 2, is an all-composite structure having wraparound fiberglass skins supported by integral fiberglass main and aft spars, whereas the current OH-58A airfoil section utilizes wraparound aluminum skins supported by a spanwise spar consisting of a 3/4-inch-wide strip of aluminum honeycomb core located at approximately 30% chord. An insight into the relative impact resistances of these two structures, both having portions of their skins unsupported, may be obtained by comparing the impact data for core-supported aluminum and fiberglass skin airfoil sections obtained from Reference 8 and presented in Figure 28. Figure 28 indicates that core-supported fiberglass skin airfoil sections will receive a shallower, wider crater (lower stress concentration) than will core-supported aluminum skins. The difference in impact resistance of these two structures is primarily attributed to the impact resistance of the skins. Limited testing of unsupported .031-inch-thick aluminum sheet, representing the unsupported skin of the present OH-58A tail rotor blade; and .021-inch-thick fiberglass sheet, representing the unsupported skin of the EPBTR, was undertaken to verify that the trends indicated by the impact data shown in Figure 28 also apply to unsupported fiberglass and aluminum skins. This testing, performed at kinetic energy levels between 103 and 250 inch-pounds, showed appreciable differences in the behavior of the two materials. The fiberglass sheet showed signs of slight crazing and no permanent deformation at the lower impact levels. At the same energy levels, however, the aluminum sheet was permanently dented. At the higher energy level of 250 inch-pounds, the depth of the dents in the aluminum increased significantly whereas only slight crazing was apparent in the fiberglass sheet. Test results performed on both supported and unsupported aluminum and fiberglass skins therefore indicate that the impact and damage resistance of fiberglass skins is superior to that of aluminum skins. Due to the improved damage resistance of the fiberglass skins, a substantial increase in blade MTBF for the EPBTR blade can be projected. For the purpose of this analysis, it is assumed the use of the EPBTR blade will reduce blade removals by 33%.

The present OH-58A tail rotor hub relies on a relatively large number of components to provide teetering capability. Teeter bearing failure and component wear and/or damage contribute substantially to the hub failure rate. The EPBTR hub - Elastic Pitch Beam Assembly has been designed to minimize the number of components, eliminate the need for teeter bearings, and minimizes maintenance requirements. Exposed portion of the EPBTR hub are relatively insensitive to damage and the portions of the Elastic Pitch Beam extending outboard from the hub are protected by the fiberglass blades. It is therefore reasonable to assume that the EPBTR hub - Elastic Pitch Beam Assembly could show a 30% increase in MTBF over that of the present hub.

Data from Reference 12, based on 29,000 flight hours show that the MTBF for the present tail rotor blade is 430.5 hours and that for the hub is 534 hours. Using the estimated improvements in MTBF, the EPBTR blades and hub would have MTBF's of 646 hours and 694 hours respectively. The combined MTBF's for the complete tail rotor assembly would then be 153.4 hours for the present rotor system and 220.4 hours for the EPBTR system.

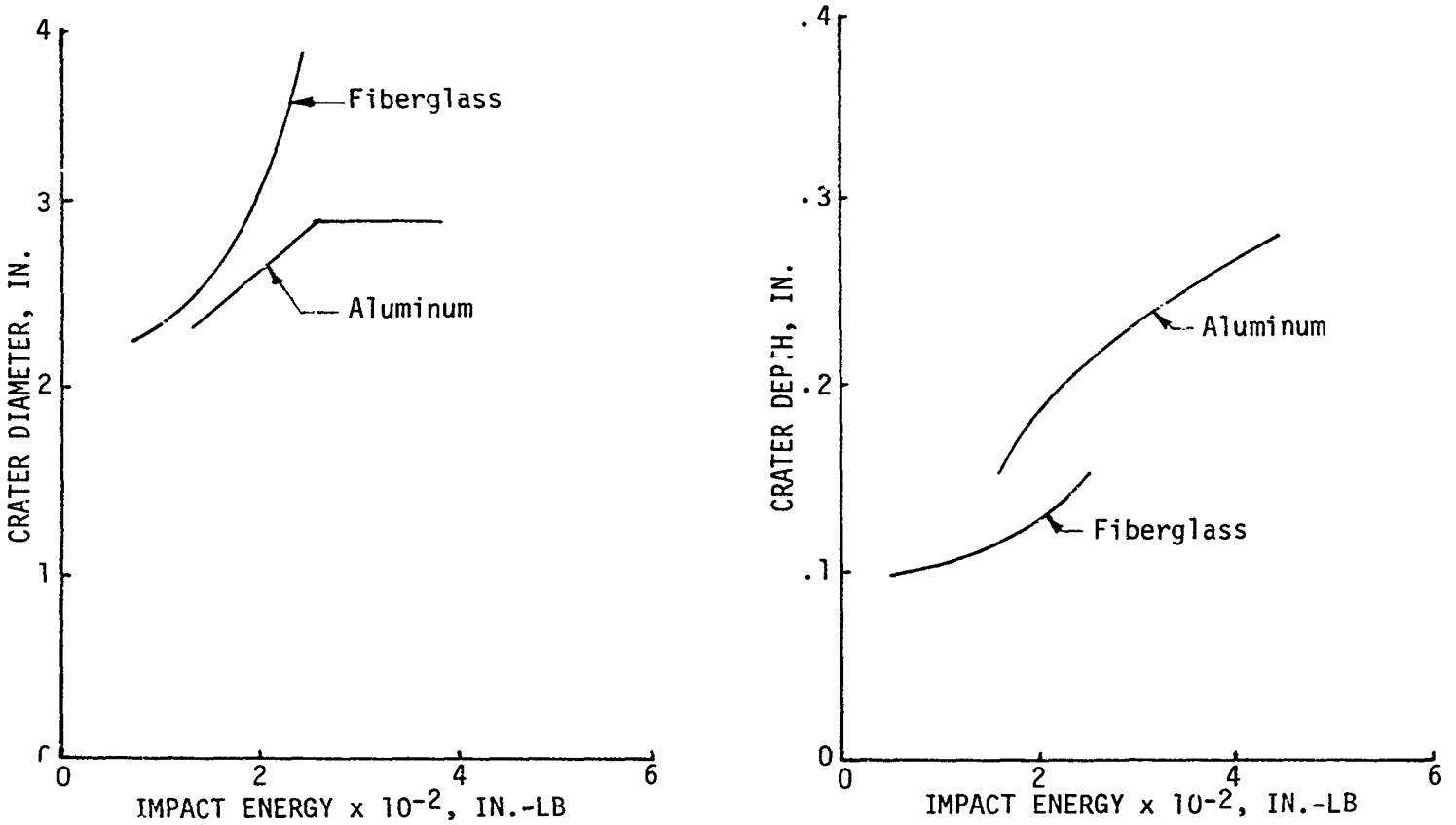

a) Crater Diameter Versus Impact Energy

b) Crater Depth Versus Impact Energy

Figure 28. Impact Resistance of Fiberglass and Aluminum Skins (Reference 8).

Experience with both the Field Repairable/Expendable Main Rotor Blade (FREB), Reference 9, and the UH-1 Elastic Pitch Beam tail rotor (UH-1 EPBTR), Reference 1, has shown the feasibility of field repairing damaged core-supported fiberglass-skinned rotor blades on the aircraft. The feasibility of repairing fiberglass-skinned structures that are unsupported by core is dependent primarily on the ability of the structure to resist bonding pressures during repair procedures without undue distortion. In the case of the OH-58A EPBTR, the increased stiffness of the leading edge portion of the blade forming a D-section with the main spar and the stiffness of the aft skin portion of the blade supported by both the main and aft spars should be adequate to resist the bonding pressure required to apply repair patches. In the event that either the main or aft spar is damaged, it is assumed that suitable reinforcing fiberglass patches may be developed to repair all but the most severe type of damage. For the purpose of the life-cycle cost analysis it is assumed that of all field repairs to the blades, approximately 70% of these will be skin repairs that are made on the aircraft and that 30% will necessitate spar-skin repairs that will be accomplished off the aircraft in the field.

Fiberglass materials are employed throughout the EPBTR blade and are far more fatigue resistant than the aluminum skins used on the present blade. This fact plus the elimination of teeter and pitch bearings to reduce possible fatigue failures associated with wear should permit appreciable increases in blade and hub fatigue lives. For the purpose of this analysis, it is assumed that the EPBTR assembly has a fatigue life of 3600 hours and, based on Reference 10 data, the fatigue life of the present rotor is assumed to be 1300 hours.

Previous experience with the Field Repairable/Expendable Main Rotor Blade (Reference 9) has shown that in the case of highly repairable fiberglass blades, the expenses incurred in maintaining a depot level of maintenance are greater than the cost of scrapping those few blades that could be repaired at depot level. It is therefore assumed that all repairs to the EPBTR will occur in the field thus eliminating the expense for depot level repair. Reference 10 indicates that a substantial number of present OH-58A blade removals were for items requiring overhaul, presumably at depot level.

Tables 6 and 7 give the life-cycle cost model output for the two tail rotors. Based upon the data from Reference 12, the present OH-58A tail rotor has a scrap rate of approximately 15%. Repair of other damage takes place either on the aircraft, off the aircraft in the field or at depot level. In the analysis of the OH-58A EPBTR, it was assumed that the current OH-58A scrappage results from severe external damage which would also cause scrappage of the EPBTR. Thus the same scrap rate of 15% was assumed for the EPBTR.

TABLE 6. LIFE-CYCLE COSTS FOR OH-58A ELASTIC PITCH BEAM TAIL ROTOR

New Rotor Price	=	$ 1431	
Mean Time Between Failures	=	220.4 Rotors Hours	
Field Repairability	=	85.0 Percent	
MEAN TIME BETWEEN MAINTENANCE ACTIONS (Rotor Hours):			
Replacements	=	1062.8	
Removals for Repair of Replacement	=	481.2	
Repairs	=	275.3	
Damage Replacements	=	1105.3	
Unscheduled Maintenance	=	220.4	
Scheduled Maintenance (Retirement)	=	27599.8	
All Maintenance Actions	=	218.7	
ROTOR EVENTS PER AIRCRAFT LIFE CYCLE:			
Number Lost to Attrition	=	0.0000	
Number Fatigue Retired Undamaged	=	0.1812	
Number Repaired on Aircraft	=	12.4773	
Number Repaired off Aircraft in Field	=	5.6852	
Number Scrapped in Field	=	3.2052	
Number Damaged and Retired in Field	=	1.3184	
Total Number Damaged and Not Repaired	=	4.5235	
Total Number All Replacements	=	4.7047	
TAIL ROTOR COSTS PER AIRCRAFT LIFE CYCLE:			
Cost of Initial Procurement:			
New Aircraft Outfitting Cost	=	$ 1431.00	
Spares Cost with Containers	=	$ 540.00	
Spare Repair Materials	=	$ 190.30	
Repair Support Equipment	=	$ 161.00	
TOTAL INITIAL PROCUREMENT COST	=		$ 2322.30
COST OF REPLACEMENT ROTORS FOR THOSE LOSE AND UNSERVICEABLE (Including Rotor Shipping and Container Shipping Costs):			
Rotors Lost to Attrition	=	$ 0.00	
Damaged Rotors Not Repaired*	=	$ 6960.10	
Time-Expired Undamaged Rotors	=	$ 282.80	
TOTAL REPLACEMENT COST	=		$ 7242.90
COST OF MAINTENANCE ACTIONS (Labor and Material to Inspect, Remove, Repair, Replace, Align, and Track):			
Field Repair on Aircraft	=	$ 2758.30	
Field Repair off Aircraft	=	$ 1098.80	
Field Scrap	=	$ 27.10	
Field Retirement	=	$ 10.10	
TOTAL MAINTENANCE COST	=		$ 3894.30
TOTAL LIFE-CYCLE ROTOR COST PER AIRCRAFT	=		$ 13459.50
MAINTENANCE MAN-HOURS/FLIGHT HOUR	=	0.0075	
ROTOR-RELATED AIRCRAFT DOWNTIME	=	35 Hours	

*Includes Spares Shipping Costs

TABLE 7. LIFE-CYCLE COSTS FOR OH-58A PRODUCTION TAIL ROTOR

New Rotor Price	=	$ 778	
Mean Time Between Failures	=	153.4 Rotor Hours	
Field Repairability	=	72.1 Percent	
MEAN TIME BETWEEN MAINTENANCE ACTIONS (Rotor Hours):			
Replacement	=	538.5	
Removals for Repair or Replacement	=	249.8	
Repairs	=	204.8	
Damage Replacements	=	611.5	
Unscheduled Maintenance	=	153.4	
Scheduled Maintenance (Retirement)	=	4513.0	
All Maintenance Actions	=	148.4	
ROTOR EVENTS PER AIRCRAFT LIFE CYCLE:			
Number Lost to Attrition	=	0.0000	
Number Fatigue Retired Undamaged	=	1.1079	
Number Repaired on Aircraft	=	13.6897	
Number Repaired off Aircraft in Field	=	8.8333	
Number Scrapped in Field	=	4.6233	
Number Damaged and Retired in Field	=	1.3559	
Number Repaired at Depot	=	1.8352	
Number Scrapped at Depot	=	1.9840	
Number Damaged and Retired at Depot	=	0.2130	
Total Number Damaged and Not Repaired	=	8.1763	
Total Number All Replacements	=	9.2842	
TAIL ROTOR COSTS PER AIRCRAFT LIFE CYCLE:			
Cost of Initial Procurement:			
New Aircraft Outfitting Cost	=	$ 778.00	
Spares Cost with Containers	=	$ 344.10	
Spare Repair Materials	=	$ 205.20	
Repair Support Equipment	=	$ 66.70	
TOTAL INITIAL PROCUREMENT COST	=		$ 1394.00
COST OF REPLACEMENT ROTORS FOR THOSE LOST AND UNSERVICEABLE (Including Rotor Shipping and Container Shipping Costs):			
Rotors Lost to Attrition	=	$ 0.00	
Damaged Rotors Not Repaired*	=	$ 7659.20	
Time-Expired Undamaged Rotors	=	$ 1006.00	
TOTAL REPLACEMENT COST	=		$ 8665.20
COST OF MAINTENANCE ACTIONS (Labor and Material to Inspect, Remove, Repair, Replace, Align, and Track):			
Field Repair on Aircraft	=	$ 375[illegible]0	
Field Repair off Aircraft	=	$ 638.10	
Field Scrap	=	$ 76.00	
Field Retirement	=	$ 35.70	
Depot Repair	=	$ 276.60	
Depot Scrap	=	$ 209.20	
Depot Retirement	=	$ 22.00	
TOTAL MAINTENANCE COST	=		$ 5015.60
TOTAL LIFE-CYCLE ROTOR COST PER AIRCRAFT	=		$ 15074.80
MAINTENANCE MAN-HOURS/FLIGHT HOUR	=	0.0147	
ROTOR-RELATED AIRCRAFT DOWNTIME	=	61 Hours	

*Includes Spares Shipping Costs

Table 8 summarizes the life-cycle cost and maintenance man-hours for the present and EPBTR rotors. As can be seen from this table, the two rotors are cost-competitive on a life-cycle basis. Additionally, since the cost of the EPBTR units could drop significantly in the near future, the EPBTR shows promise of becoming highly cost effective in reductions of not only maintenance man-hours per flight hour and rotor related aircraft downtime, but also overall life-cycle costs.

TABLE 8. LIFE-CYCLE COST AND MAINTENANCE MAN-HOUR SUMMARY

Item	Life-Cycle Cost, $	Maintenance Man-Hour Per Flight Hour	Maintenance-Related A/C Downtime, Hour
Present Tail Rotor	15,074.80	.0147	61
EPBTR Blade Hub and Elastic Pitch Beam Assembly	13,459.50	.0075	35

CONCLUSIONS

1. The feasibility of designing an Elastic Pitch Beam tail rotor for the OH-58A helicopter having reliability, maintainability, repairability, and performance that are improved over the current design has been demonstrated.

2. Static test of the Elastic Pitch Beam fabricated for this program indicates that the attachment design of the Elastic Pitch Beam to the airfoil section is more than adequate for the ultimate loading condition anticipated for this structure.

3. The fatigue life of the current OH-58A tail rotor shaft will be reduced somewhat by the elimination of teeter freedom in the LOH Elastic Pitch Beam tail rotor design.

RECOMMENDATIONS

It is recommended that:

1. Fabrication of the LOH Elastic Pitch Beam tail rotor for the OH-58A helicopter be pursued with the objective of obtaining a flightworthy tail rotor system for this aircraft.

2. Further effort be made to reduce the vibratory hub moment being transferred to the current OH-58A tail rotor shaft and/or to redesign the shaft to increase its fatigue capabilities for this type of loading.

REFERENCES

1. Maloney, P.F., ELASTIC PITCH BEAM FLIGHT SAFETY DATA, KAC Report R-1286, Kaman Aerospace Corporation; USAAMRDL Contract DAAJ02-72-C-0006, ELASTIC PITCH BEAM TAIL ROTOR, U.S. Army Air Mobility Research and Development Laboratory, Fort Eustis, Virginia, July 19, 1974.

2. Falcone, A.S., Clark, F., and Maloney, P., ELASTIC PITCH BEAM TAIL ROTOR OPERATIONAL SUITABILITY INVESTIGATION, Kaman Aerospace Corporation; USAAMRDL Technical Report TR-74-60, Eustis Directorate, U.S. Army Air Mobility Research and Development Laboratory, Fort Eustis, Virginia, July 1974, AD 784595.

3. ELASTIC PITCH BEAM TAIL ROTOR STUDY FOR LOH CLASS HELICOPTERS, Kaman Aerospace Report Number R-1325, Kaman Aerospace Corporation; USAASC Contract DAAJ01-73-C-0282(P3L) ELASTIC PITCH BEAM TAIL ROTOR STUDY FOR LOH CLASS HELICOPTERS, U.S. Army Aviation Systems Command, St. Louis, Missouri, February 1975.

4. Anon, MILITARY STANDARDIZATION HANDBOOK, METALLIC MATERIALS AND ELEMENTS FOR AEROSPACE VEHICLE STRUCTURES, MIL-HDBK-5B, Department of Defense, Washington, D.C., 1 September, 1975.

5. Anon, PLASTICS FOR AEROSPACE VEHICLES, PART 1. REINFORCED PLASTICS, MIL-HDBK-17A, Department of Defense, Washington, D.C., January 1971

6. Werren, F., SUPPLEMENT TO FATIGUE TESTS OF GLASS FABRIC BASE LAMINATES SUBJECTED TO AXIAL LOADING, Forest Products Laboratory; FPL Report No. 1823-B, Forest Service, U.S. Department of Agriculture, Washington, D.C., August 1956.

7. Peterson, R.E., STRESS CONCENTRATION DESIGN FACTORS, New York, N.Y., John Wiley & Sons, Inc., October 1953.

8. Maloney, Paul F., et al, PRELIMINARY DESIGN STUDY OF IMPROVED ROTOR BLADE FOR AH-1Q HELICOPTER, Kaman Final Technical Report No. R-1314, Kaman Aerospace Corporation; USAAMRDL Contract DAAJ02-75-C-0008, U.S. Army Air Mobility Research and Development Laboratory, Fort Eustis, Virginia, January 1975.

9. Frengley, Michael C., DEVELOPMENT PROGRAM FOR FIELD-REPAIRABLE/ EXPENDABLE MAIN ROTOR BLADES, PHASE I - PRELIMINARY DESIGN, Kaman Aerospace Corporation; USAAMRDL Technical Report TR-73-102, Eustis Directorate, U.S. Army Air Mobility Research and Development Laboratory, Fort Eustis, Virginia, April 1974, AD 783444.

10. MAJOR ITEM SPECIAL STUDY, OH-58A Tail Rotor Blade, FSN 16151216545, PN 2060107505, A Reliability and Maintainability Management Improvement Techniques Report, Period Covered by Data January 1, 1968 Thru July 1, 1971, Directorate for Product Assurance, U.S. Army Aviation Systems Command, St. Louis, Missouri 63166.

11. Knudsen, George E., and Carr, Patricia V., R&M DATA ANALYSIS OF THE UH-1/AH-1 TAIL ROTOR SYSTEM, Bell Helicopter Company; USAAMRDL Technical Report TR-74-11, Eustis Directorate, U.S. Army Air Mobility Research and Development Laboratory, Fort Eustis, Virginia, April 1974, AD 782858.

12. Cook, T. Young, R., and Starses, F., MAINTAINABILITY ANALYSIS OF MAJOR HELICOPTER COMPONENTS, Kaman Aerospace Corporation; USAAMRDL Technical Report TR-73-43, Eustis Directorate, U.S. Army Air Mobility Research and Development Laboratory, Fort Eustis, Virginia, August 1973.

LIST OF SYMBOLS

A	area of cross section, $in.^2$
A_{bd}	doubler bond area, $in.^2$
A_{bL}	laminate bond area, $in.^2$
A_{br}	bearing area, $in.^2$
A_s	shear area, $in.^2$
A_t	tensile area, $in.^2$
C	distance from neutral axis to given point, in.
C_x	x-distance from neutral axis to given point, in.
C_y	y-distance from neutral axis to given point, in.
CF	centrifugal force, lb
d, D	diameter, in.
e	hinge offset, in.
E	modulus of elasticity, psi
EA	axial stiffness, lb
EI_{xx}	bending stiffness about x-axis, $lb\text{-}in.^2$
EI_{yy}	bending stiffness about y-axis, $lb\text{-}in.^2$
f	stress, psi
f_b	bending stress or combined stress, psi
f_{bru}	ultimate bearing stress, psi
f_{ib}	interface bond stress, psi
f_{ibu}	ultimate interface bond stress, psi
f_s	shear stress or steady stress, psi
f_{su}	ultimate shear stress, psi
f_t	tensile stress, psi

f_{tu}	ultimate tensile stress, psi
f_v	vibratory stress, psi
F_a	allowable vibratory stress, psi
F_e	endurance limit, psi
F_{bru}	allowable ultimate bearing stress, psi
F_{su}	allowable ultimate shear stress, psi
F_{tu}	allowable ultimate tensile stress, psi
I	moment of inertia, $in.^4$
I_{xx}	moment of inertia about x-axis, $in.^4$
I_{yy}	moment of inertia about y-axis, $in.^4$
K_t	theoretical stress concentration factor
$K_{\beta e}$	experimentally measured flapping spring rate, in.-lb/deg
$K_{\beta t}$	theoretical flapping string rate, in.-lb/deg
K_θ	torsional stiffness about pitch axis, in.-lb/deg
L	length, in.
M	moment, in.-lb
M_x	moment about x-axis, in.-lb
M_y	moment about y-axis, in.-lb
M_H	hub moment, in.-lb
MS_{bru}	ultimate margin of safety in bearing
MS_f	margin of safety in fatigue
MS_{su}	ultimate margin of safety in shear
MS_{tu}	ultimate margin of safety in tension
P_d	load in doubler, lb
P_{du}	ultimate load in doubler, lb

P_L	load in laminate, lb
P_{Lu}	ultimate load in laminate, lb
P_u	ultimate load, lb
R_x	reaction in x-direction, lb
R_y	reaction in y-direction, lb
R_R	resultant reaction, lb
t	thickness, in.
t_L	laminate thickness, in.
T	torque, in.-lb
V	shear, lb
X_{cg}	x-distance to centroidal axis measured from reference, in.
X_{NA}	x-distance to neutral axis measured from reference, in.
Z	flapping spring rate corrector
β	flapping angle, deg
δ	deflection, in.
θ	pitch angle, deg
Σ	summation
λ	$(CF/EI_{XX})^{\frac{1}{2}}$, 1/in.